(Nitta Gelatin, Osaka, Japan). After 30 minutes of incubation at 37°C on basal layer collagen, 1 or 2 × 10^4 cells were suspended in 1 mL Dulbecco's modified Eagle's medium (DMEM)/F12 mixed with 1 mL collagen gel solution and plated onto basal layer collagen in six-well culture dishes. Plated cells were cultured for 7 days with an additional 2 mL DMEM supplemented with 10% fetal calf serum (FCS) (Sigma, St. Louis, MO), 1× insulin/transferrin/selenium, 20 ng/mL epidermal growth factor (EGF, PeproTech, Rocky Hill, NJ), 20 ng/mL hepatocyte growth factor (HGF, PeproTech), and 25 ng/mL tumor necrosis factor α (PeproTech).

In Vitro *Bile Duct–Like Differentiation Assay of Hepatic Progenitor Cell Line.* The HPPL liver progenitor cell line has been reported to exhibit characteristics of differentiated cholangiocytes in three-dimensional culture.[18,19] As in the previous report, we maintained HPPL cells in DMEM/F12 containing 10% FCS, 1× insulin/transferrin/selenium, 10 mM nicotinamide, 10^{-7} M Dex, and 5 ng/mL HGF and EGF and suspended cells in a mixture of type I collagen and Engelbreth-Holm-Swarm (EHS) sarcoma gel (Becton Dickinson, Bedford, MA) at a density of 4 × 10^4 cells/mL. Cell suspension was added to each cell culture insert (Millipore, Billerica, MA) and after incubation at 37°C for 2 hours, 500 μL of DMEM/F12 with growth factors was added above and below the insert, and the cells were cultured for 7 days. To test the effects of inhibitors of CaMKII, Rho-kinase, Rac1, calcineurin, and PKC on HPPL differentiation, KN93, KN92, KN62, Y-27632, NSC23766, cyclosporin A, and Go6976 (Supporting Information) were added individually to the culture medium when each three-dimensional culture was initiated. Independent analyses were performed in triplicate, and five fields were randomly selected for counting the cysts that indicate bile duct–like differentiation of cells.

In Vitro *Hepatic Maturation Assay of Primary Hepatoblasts.* To induce hepatic differentiation, primary hepatoblasts from WT E14.5 mice were cultured as described.[6] Briefly, 2.5 × 10^5 magnetic cell sorter–isolated Dlk^+ cells were cultured in DMEM supplemented with 10% FCS, 2 mM L-glutamine, 1× nonessential amino acid, 100 U/mL penicillin, 100 μg/mL streptomycin, and 10^{-7} M Dex in each well of a six-well gelatin-coated dish. After 5 days, the resulting cells were supplemented with medium containing 20% EHS gel for an additional 2 days prior to analysis.

Details regarding materials, cell isolation, hematoxylin and eosin staining, reverse-transcriptase polymerase chain reaction (RT-PCR) analysis, immunostaining, immunoblot analysis, Wnt5a-blocking experiments, microarray analysis, and statistical analysis are described in the Supporting Information.

Results

Expressions of Wnt5a and Frizzled Receptors During Liver Development. We first analyzed *Wnt5a* expression during liver development using quantitative RT-PCR. *Wnt5a* expression was detected in fetal and neonatal livers of WT mice and showed a gradual increase during liver development (Fig. 1A). To investigate Wnt5a expression in midgestational fetal liver, we purified the fractions of hepatoblasts, mesenchymal cells, mesothelial cells, endothelial cells, and hematopoietic cells from E14.5 liver using FACS. Quantitative RT-PCR analysis indicated that *Wnt5a* was expressed in hepatoblasts, mesenchymal cells, mesothelial cells, endothelial cells, and hematopoietic cells. The expression level of Wnt5a was significantly higher in mesenchymal cells than in hepatoblasts and other types of cells in midgestational fetal liver (Fig. 1B). Frizzled is a family of cell surface receptors for Wnt ligands. Adult hepatocytes from 12-week-old mice served as the control. RT-PCR analysis of E14.5 hepatoblasts resulted in the detection of 9 of 10 Fzd receptors (all except *Fzd9*), whereas E14.5 hematopoietic cells expressed 9 of 10 Fzd receptors (all except *Fzd2*) (Fig. 1C and Supporting Fig. 1).

Loss of Wnt5a Promotes the Formation of Bile Duct in Fetal Liver. Because one of the reported phenotypes of systemic Wnt5a KO mice was postpartum death,[11] we investigated the function of Wnt5a in liver development using mid- to late gestational fetuses. We determined that although average liver weight in Wnt5a KO E18.5 fetal mice was significantly lower than in WT littermates, the average liver/body weight ratio in KO mice was not significantly different from the ratio in WT mice (Supporting Fig. 2).

Histological analysis of E18.5 livers showed that the number of luminal spaces around the portal vein, which we interpret to be primitive bile ducts, was greater in Wnt5a KO mice than in WT mice (Fig. 2A). To further investigate these changes in bile duct development, expression of *Sox9* (a representative transcriptional factor expressed in biliary precursor cells)[20] was analyzed. Expression levels of *Sox9* were significantly higher in Wnt5a KO E16.5 fetal livers relative to WT livers (Fig. 2B). The Notch pathway plays an essential role in the morphogenesis of bile duct structures.[21] Expression levels of *Notch1*, *Notch2*, and

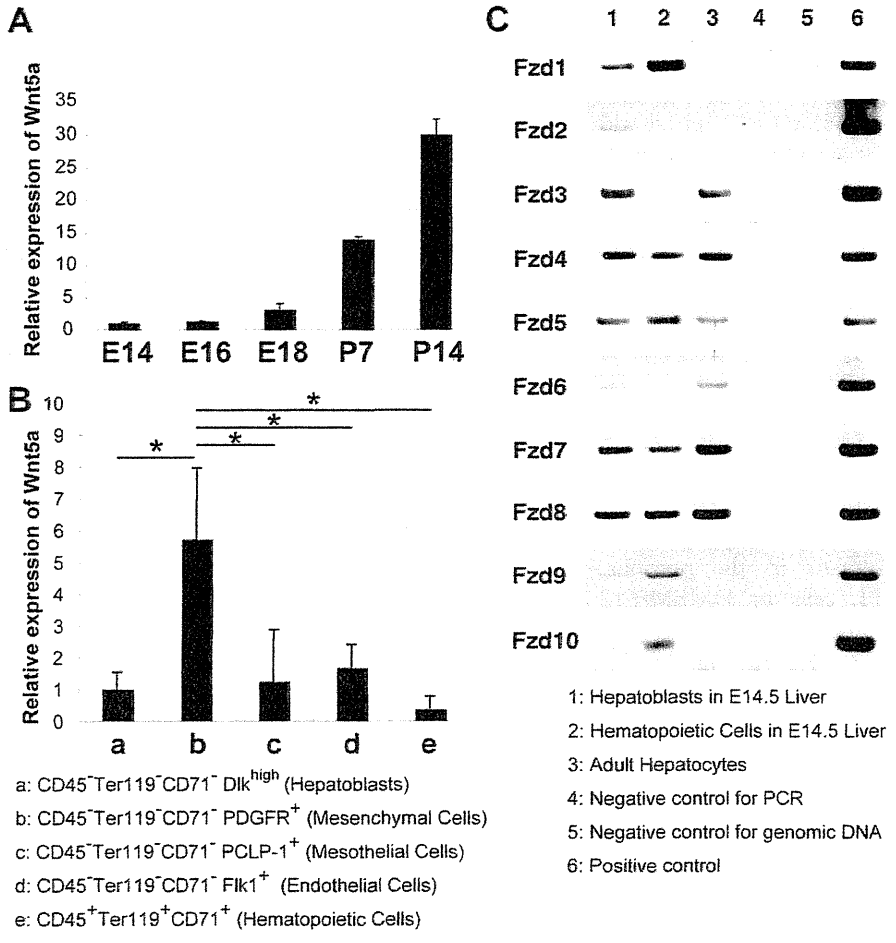

Fig. 1. Expression analyses of Wnt5a and Fzd receptors during liver development. (A) Quantitative RT-PCR analysis of Wnt5a in fetal and neonatal livers. E14, E16, E18, P7, and P14 indicate Wnt5a expression in whole livers derived from WT mice at these days of development, respectively. Values represent the ratio of Wnt5a at each stage relative to expression of this RNA in E14.5 fetal liver following normalization of template copy number to β-actin. Bars represent the mean ± SD of three separate experiments. (B) Quantitative RT-PCR analysis of Wnt5a. Lane a: $CD45^-Ter119^-CD71^-Dlk^{high}$ cells from E14.5 liver (hepatoblasts). Lane b: $CD45^-Ter119^-CD71^-PDGFR^+$ cells from E14.5 liver (mesenchymal cells). Lane c: $CD45^-Ter119^-CD71^-PCLP\text{-}1^+$ cells from E14.5 liver (mesothelial cells). Lane d: $CD45^-Ter119^-CD71^-Flk1^+$ cells from E14.5 liver (endothelial cells). Lane e: $CD45^+Ter119^+CD71^+$ cells from E14.5 liver (hematopoietic cells). All lanes were normalized by numbers of β-actin copies quantified by TaqMan-PCR analysis; equal numbers of copies were applied as templates. Wnt5a expression was significantly higher in mesenchymal cells than in hepatoblasts, mesothelial cells, endothelial cells and hematopoietic cells. Bars represent the mean ± SD of three separate experiments. $*P < 0.05$. (C) Expression of Fzd family. Lane 1: hepatoblasts ($CD45^-Ter119^-Dlk^{high}$ cells) purified from E14.5 liver. Lane 2: hematopoietic cells ($CD45^+Ter119^+$ cells) from E14.5 liver. Lane 3: adult hepatocytes from 12-week-old mouse liver. Lane 4: negative control (distilled water). Lane 5: samples without reverse-transcriptase reaction (negative controls for false-positive amplification of genomic DNA). Lane 6: positive control. RT-PCR products of Fzd receptors are indicated. Images shown are representative of three separate experiments.

Jagged1 were significantly higher in Wnt5a KO E16.5 fetal livers relative to WT livers (Supporting Fig. 3A). Numbers of $Hes1^+$ cells in E18.5 livers were significantly greater in Wnt5a KO mice than in WT mice (Supporting Fig. 3B). Expression levels of *Cyclin D1* and *c-Myc* (target transcripts of canonical β-catenin–dependent Wnt pathway) in Wnt5a KO livers were equal to those in WT livers (Supporting Fig. 4A). We tried to assess the protein level of Sox9; however, immunostaining analysis of Sox9 did not work well, probably due to technical problems (data not shown).

During normal liver development, hepatoblasts located around the portal vein develop as hepatocyte nuclear factor (HNF) $1\beta^+HNF4\alpha^-$ biliary precursor cells.[22] In normal E16.5 fetal livers, monolayer rings of biliary precursor cells, termed ductal plates, can be detected.[23] WT E18.5 fetal livers contained primitive ductal structures (PDSs) consisting of multiple $HNF1\beta^+$ cytokeratin $(CK)19^+$-cell lumina (Fig. 2C).

Immunohistological analysis revealed that numbers of $HNF1\beta^+HNF4\alpha^-$ biliary precursor cells in E16.5 livers (Fig. 2D) and in PDSs formed by these cells in

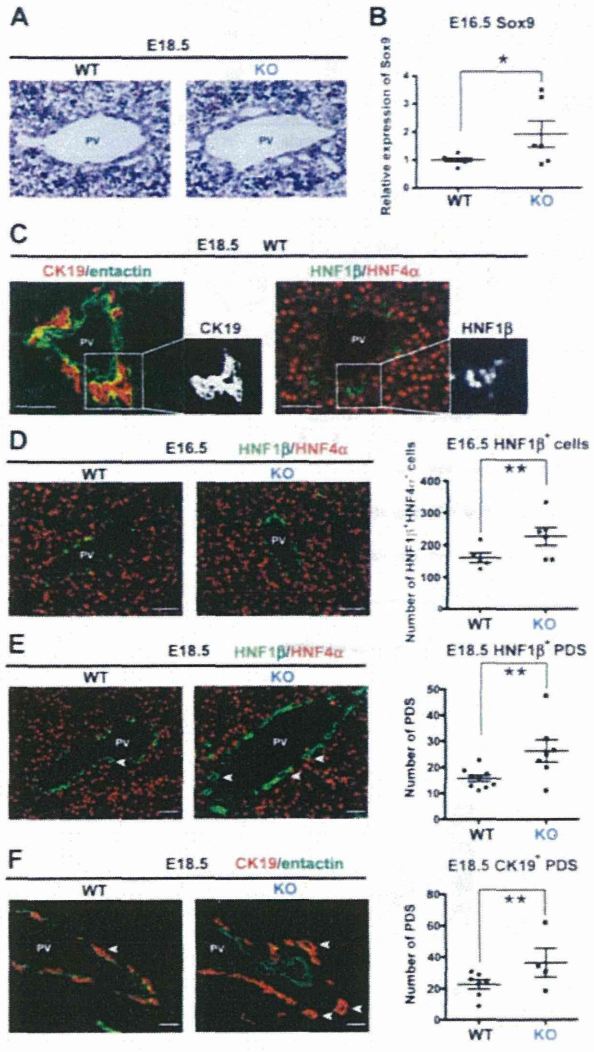

Fig. 2. Loss of Wnt5a excessively promotes the formation of bile duct in fetal liver. (A) Representative images depicting luminal spaces around the portal vein (PV) in E18.5 Wnt5a KO and littermate WT livers stained with hematoxylin and eosin. (B) Quantitative RT-PCR analysis of the cholangiocyte marker Sox9 is depicted as the ratio of Sox9 copy number in E16.5 Wnt5a KO livers relative to WT livers (all normalized to β-actin). Steady-state levels of Sox9 mRNA were significantly higher in Wnt5a KO livers relative to WT livers. $^*P < 0.05$. (C) Representative images of immunostained sections from E18.5 WT livers. Left panel: double immunostaining using CK19 (red) and entactin (green) antibodies. Right panel: double immunostaining using HNF1β (green) and HNF4α (red) antibodies. Insets depict high-power field images of cells with positive staining for CK19 (left panel) and HNF1β (right panel). PV, portal vein. (D, E) Left two panels: immunostaining of HNF1β (green) and HNF4α (red) in E16.5 (D) and E18.5 (E) livers. Right panel (D): number of HNF1β^+HNF4α^- cells in 10 random fields examined in WT and Wnt5a KO livers. Right panel (E): number of primitive ductal structures (PDSs) in 10 random fields examined in WT and Wnt5a KO livers. PV, portal vein. (F) Left panel: immunostaining of CK19 (red) and entactin (green) in E18.5 livers. Right panel: numbers of PDSs in 10 random fields of WT and Wnt5a KO livers. Arrowheads indicate PDSs. PV, portal vein. Images shown are representative of three independent experiments. Bars in dot-plot graphs represent mean ± SEM of values shown. $^{**}P < 0.01$. Scale bars: 50 μm.

E18.5 livers (Fig. 2E) were significantly higher in Wnt5a KO mice relative to WT mice. Double staining of CK19 and entactin (a component of basement membrane) confirmed that the number of PDSs formed by CK19$^+$ cells was also significantly higher in E18.5 Wnt5a KO liver relative to WT liver (Fig. 2F). These results demonstrate clearly that loss of Wnt5a excessively promotes the formation of bile ducts in fetal liver.

Expression Analysis of Fetal Livers in Wnt5a KO Mice. Expression of genes coincident with hepatic maturation was also analyzed in Wnt5a KO fetal livers using quantitative RT-PCR. In E16.5 fetal livers, albumin (ALB) and HNF4α messenger RNA (mRNA) levels were nearly equal between WT and Wnt5a KO mice. Similarly, we observed no significant differences between WT and Wnt5a KO E18.5 fetal livers with regard to copy numbers of tyrosine aminotransferase, carbamoyl phosphate synthetase 1 (CPS1), glucose 6-phosphatase (G6Pase), or HNF4α mRNAs (Supporting Figs. 5A and B). These data suggest that the maturation of hepatoblasts to hepatocytes is not impaired in Wnt5a KO mice.

Proliferation of fetal liver cells in Wnt5a KO mice was analyzed by immunoblot and immunostaining. Immunoblot analysis revealed that proliferating cell nuclear antigen (PCNA) production in Wnt5a KO livers was almost equal to that in WT livers (Supporting Fig. 4B). Numbers of CK19$^+$PCNA$^+$ cells in E18.5 were almost equal to those in WT livers (Supporting Fig. 4C). Changes in gene expression in Wnt5a KO livers were analyzed using complementary DNA microarray analysis (Supporting Fig. 5C and Supporting Table 5). Cluster analysis revealed that several molecules associated with amino acid metabolism and cell migration were up-regulated or down-regulated in Wnt5a KO fetal livers compared with those in WT livers.

Wnt5a Retards Formation of Bile Duct–Like Structures from Primary Hepatoblasts. In collagen gel-embedding culture, mouse primary hepatoblasts differentiate into bile duct–like branching structures, coincident with the expression of biliary cell-specific genes such as CK19 (Fig. 3A, left panel).[6] To investigate the effects of Wnt5a on differentiation of hepatoblasts into biliary cells *in vitro*, we cultured primary hepatoblasts derived from E14.5 WT fetal livers and assessed the formation of bile duct–like branching structures.

We observed that cells in cultures derived from E14.5 WT fetal liver formed approximately 10 colonies (consisting of >100 cells in large branching structures) per 1×10^4 cells (Fig. 3A, right panel); colonies with

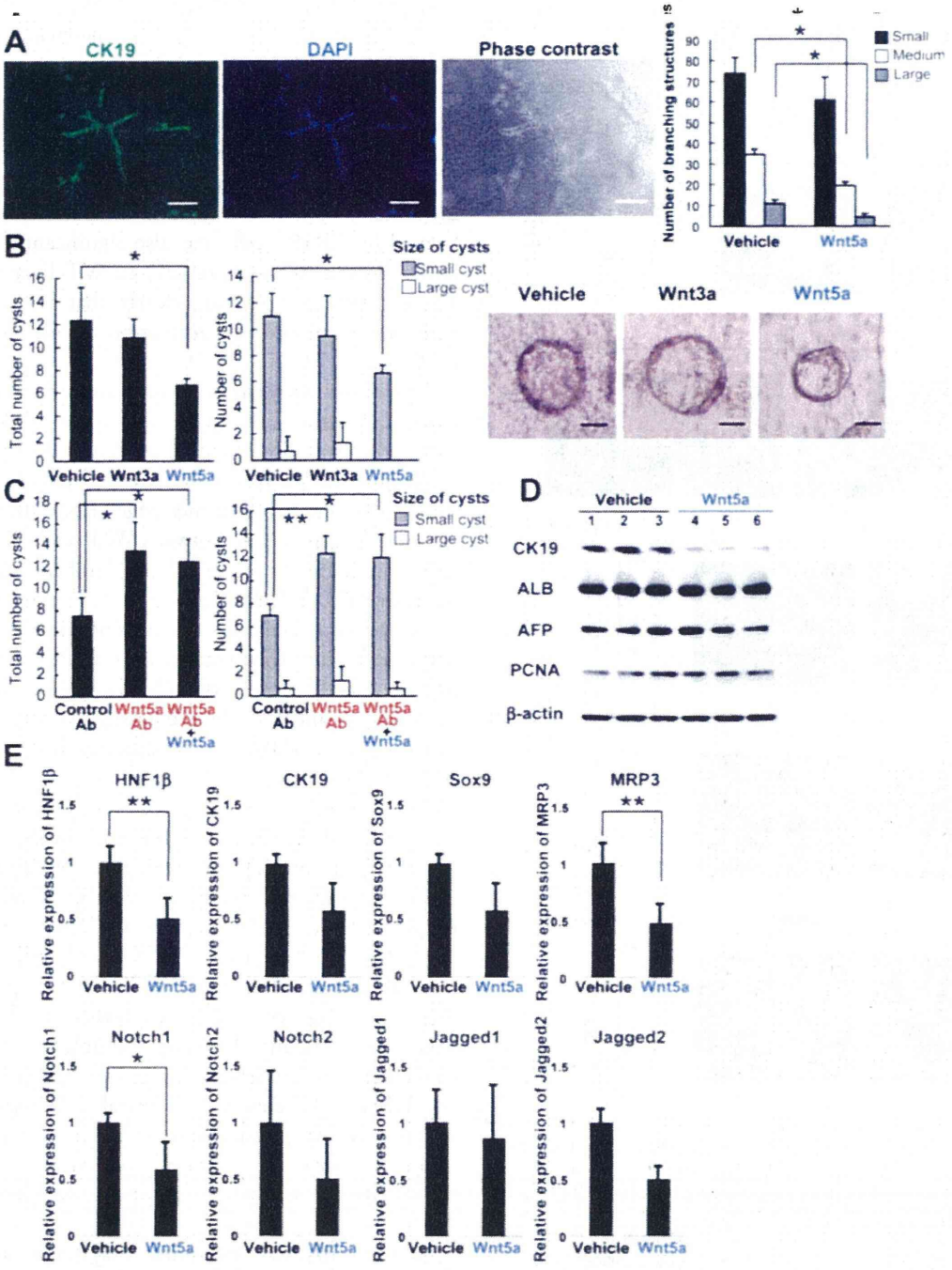

Fig. 3. Wnt5a suppresses formation of bile duct-like structures derived from hepatic stem/progenitor cells. (A) Bile duct-like branching structures derived from primary hepatoblasts. Left panel: representative view of bile duct-like branching structures consisting of >100 cells derived from primary hepatoblasts. Colonies were immunostained with CK19 (green) and counterstained with 4',6-diamidino-2-phenylindole (DAPI) (blue). Scale bar: 100 μm. Right panel: numbers of colonies demonstrating branching structures in cultures supplemented with 100 ng/mL Wnt5a or vehicle only. Numbers of small (consisting of 10-49 cells), medium-sized (50-99 cells), and large (>100 cells) branching structures per one well were counted. *$P < 0.05$. (B) Numbers of bile duct-like cysts derived from the hepatic stem/progenitor cell line (HPPL) in five random fields per well in cultures supplemented with 100 ng/mL Wnt5a, 100 ng/mL Wnt3a, or vehicle only (left panel). There were significantly fewer small cysts (50-100 μm diameter with clear lumina) and large cysts (diameter >100 μm with clear lumina) in cultures supplemented with Wnt5a relative to vehicle only. Right panel: representative views of cysts in HPPL three-dimensional cultures supplemented with either vehicle, Wnt3a or Wnt5a. Scale bars: 50 μm. *$P < 0.05$. (C) Numbers of bile duct-like cysts derived from HPPL in five random fields per well in cultures supplemented with either control immunoglobulin G, anti-Wnt5a Ab, or both anti-Wnt5a Ab plus recombinant Wnt5a protein. Cultures treated with anti-Wnt5a Ab resulted in a significant increase in total numbers of bile duct-like cysts derived from HPPL, and blocked the effect of Wnt5a supplementation. *$P < 0.05$. **$P < 0.01$. (D) Immunoblot analysis of CK19, ALB, AFP, and PCNA in HPPL-derived cysts treated with Wnt5a. CK19 production in HPPL-derived cysts treated with Wnt5a was down-regulated relative to that with vehicle-supplemented controls, whereas protein levels of ALB, AFP, and PCNA did not change. Lanes 1-3 and lanes 4-6 are vehicle-supplemented controls and Wnt5a-supplemented HPPL-derived cysts, respectively. (E) Expression analysis of HPPL-derived cysts treated with Wnt5a. Expression levels of HNF1β, MRP3, and Notch1 in HPPL-derived cysts in medium supplemented with Wnt5a were significantly lower than those in HPPL-derived cysts in medium supplemented with vehicle, indicating that Wnt5a retarded biliary maturation of HPPL cysts. Results represent the mean ± SD of three separate experiments. *$P < 0.05$. **$P < 0.01$.

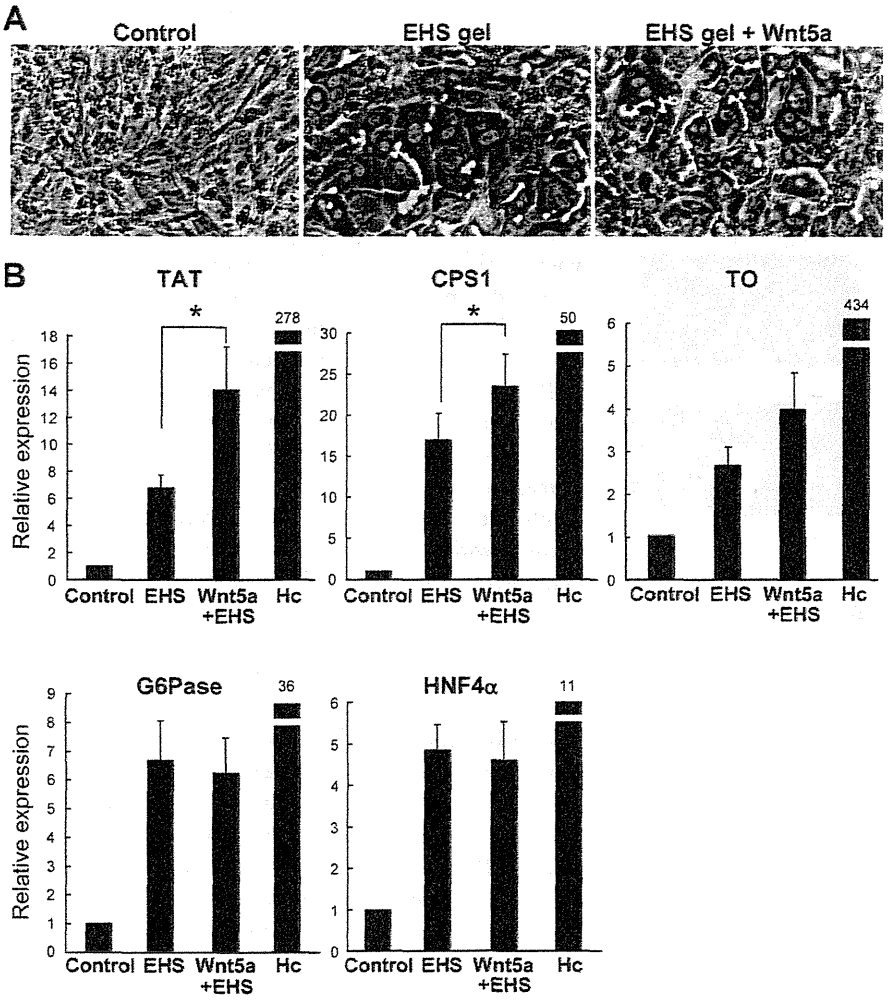

Fig. 4. Expression of hepatic maturation markers under culture supplemented with Wnt5a. (A) Phase contrast images of cultured primary hepatoblasts induced to mature to hepatocytes with EHS gel alone or EHS gel plus 100 ng/mL Wnt5a. (B) Expression levels of tyrosine amino transferase (TAT), CPS1, tryptophan-2,3-oxygenase (TO), G6Pase, and HNF4α are depicted as the ratio of copy mRNA number in cells treated with EHS gel alone or EHS gel plus 100 ng/mL Wnt5a for 7 days relative to control cells. Hc, primary adult hepatocytes from 12-week-old mice (positive control). All samples were normalized by numbers of β-actin copies quantified by TaqMan-PCR analysis; equal numbers of copies were applied as templates. Results represent the mean ± SD of three independent experiments. $*P < 0.05$.

medium (50-99 cells) or small (10-49 cells) branching structures also were noted. In cultures supplemented with Wnt5a, there were significant decreases in the average number colonies with large- and medium-sized branching structures relative to vehicle-only controls.

Wnt5a Suppresses Cyst Formation Derived from HPPL in Three-Dimensional Culture. To assess the potential of hepatic stem/progenitor cells for bile duct–like luminal formation, we used an HPPL three-dimensional culture system.[19] HPPL is established from mouse E14 Dlk^+ hepatoblasts and differentiates into hepatic and cholangiocytic lineages.[18] In this system, HPPL cells form cysts that exhibit characteristics of differentiated cholangiocytes producing CK19, E-cadherin, and other characteristic markers. We categorized HPPL-derived colonies into one of three classes: colonies without clear lumina, small cysts (50-100 μm diameter with clear lumina), and large cysts (>100 μm diameter with clear lumina). As described,[19] immuno-cytostaining of cultured cells showed that colonies without clear lumina produced both the hepatic marker ALB and the biliary marker CK19, suggesting incomplete terminal differentiation. Cells in the luminal walls of small and large cysts, in contrast, produced CK19 but not ALB, indicating their differentiation to a cholangiocyte lineage (Supporting Fig. 6). Vehicle-only controls or cultures treated with Wnt3a did not show a significant difference in overall number of cysts. In contrast, cultures supplemented with Wnt5a displayed significantly fewer cysts, due both to an absence of large cysts and a significantly reduced number of small cysts (Fig. 3B). Wnt5a is expressed in HPPL cells (Supporting Fig. 7A). We verified the specificity of effect of Wnt5a by blocking experiments. Cultures supplemented with anti-Wnt5a antibody (Ab) resulted in a significant increase in numbers of HPPL-derived cysts relative to control Ab, and

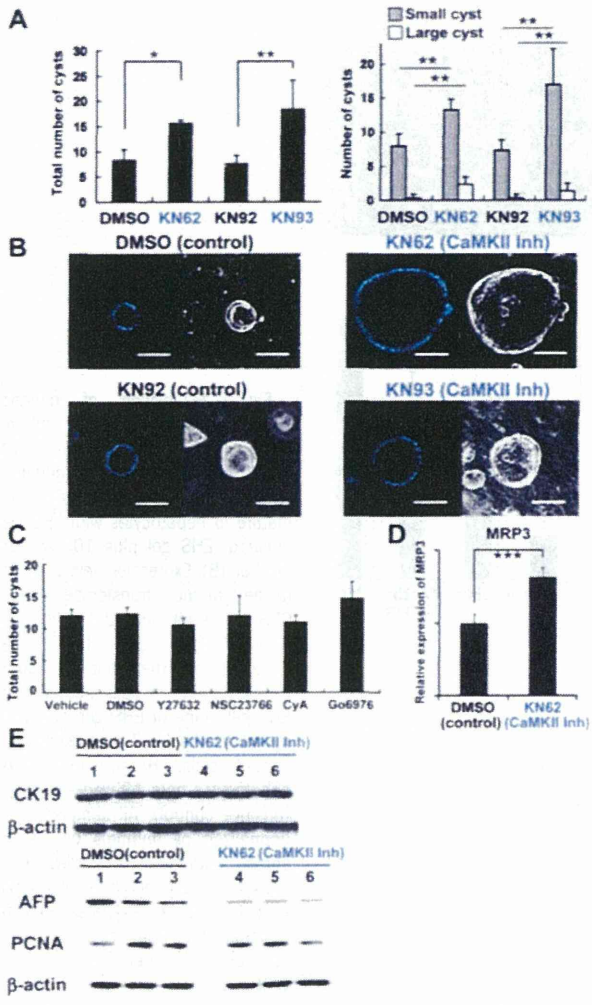

Fig. 5. Inhibitors of CaMKII increased the number and size of bile duct-like cysts derived from HPPL. (A) Inhibitors specific for CaMKII activity (KN62 and KN 93) were added at the beginning of HPPL three-dimensional culture. Numbers of total cysts, small cysts, and large cysts increased significantly in medium supplemented with KN62 or KN93. Cultures treated with dimethyl sulfoxide (DMSO) alone (vehicle) or KN92 (an inactive analogue of KN93) served as negative controls for KN62 (vehicle) and KN93, respectively. $*P < 0.01$. $**P < 0.05$. (B) Representative DAPI-stained (blue, left panels) or phase contrast confocal microscopy images (right panels) of bile duct-like cysts. Scale bars: 100 μm. (C) Numbers of total cysts were not changed by the inhibitors of Rho kinase (Y-27632), Rac1 (NSC23766), calcineurin (cyclosporin A [CyA]), or PKC (Go6976). Vehicle-only treatments (distilled water or DMSO) served as negative controls for Y-27632 (in distilled water), NSC23766 (in distilled water), CyA (in DMSO), and Go6976 (in DMSO). (D) Expression of MRP3 in HPPL cysts. MRP3 expression was significantly increased in medium supplemented with CaMKII inhibitor (KN62), suggesting that CaMKII inhibitor promoted biliary maturation of HPPL cysts. $***P < 0.01$. (E) Immunoblot analysis of CK19, AFP, and PCNA in HPPL-derived cysts treated with vehicle (DMSO) or CaMKII inhibitor (KN62). The level of AFP in HPPL-derived cysts treated with CaMKII inhibitor was lower than that in vehicle-supplemented controls, whereas the levels of CK19 and PCNA did not change. Results represent the mean ± SD of three independent experiments.

blocked the effects of Wnt5a supplementation (Fig. 3C). Numbers of HPPL-derived cysts were higher in cultures supplemented with Wnt5a-specific inhibitor relative to vehicle-only controls (Supporting Fig. 7B).

Immunoblot analysis indicated that CK19 production in HPPL-derived colonies were significantly down-regulated in cultured cells supplemented with Wnt5a relative to vehicle-supplemented controls, whereas the levels of ALB, α-fetoprotein (AFP), and PCNA did not change (Fig. 3D). Expression analysis of HPPL-derived colonies revealed that HNF1β, Notch1, and multidrug resistance–associated protein 3 (MRP3, a key primary active transporter in biliary cells) were significantly down-regulated in cultured cells supplemented with Wnt5a relative to vehicle-supplemented controls (Fig. 3E). HNF1β and Sox9 were significantly up-regulated in cultured cells supplemented with anti-Wnt5a Ab relative to control Ab (Supporting Fig. 7C), whereas the levels of hepatocytic markers did not change (Supporting Fig. 7D). Consistent with our *in vivo* results, these data indicate that Wnt5a suppresses bile duct–like cyst formation of fetal hepatic progenitor cells *in vitro*.

***Wnt5a Induces the Expression of Hepatic Maturation Markers in Primary Hepatoblasts* In Vitro.** We evaluated the potential of primary hepatoblasts for hepatic maturation using an *in vitro* hepatic differentiation assay.[24] Phase-contrast microscopy after addition of EHS gel identified several morphological changes within cells, including formation of highly condensed cytosol, and clear, round nuclei typical to mature hepatocytes (Fig. 4A, middle panel). Because similar gross morphological changes were also seen in cells cultured in the presence of Wnt5a (right panel), we used quantitative RT-PCR to measure the effect of Wnt5a on expression of hepatic maturation marker genes in stem/progenitor cells. Expression of tyrosine aminotransferase and CPS1 in cultured cells increased significantly with supplemental Wnt5a (Fig. 4B), whereas changes in tryptophan-2,3-dioxygenase, G6Pase, and HNF4α mRNA levels were not significantly different. These results indicate that Wnt5a contributes, in part, to primary hepatoblast maturation. Taken together, our *in vitro* data demonstrate that Wnt5a retards biliary differentiation and promotes hepatic differentiation of hepatoblasts.

Inhibition of CaMKII Activity Promotes the Formation of Bile Duct–Like Cysts Derived from HPPL. While Wnt5a is known to stimulate several signaling cascades, including CaMKII, Rho-kinase, Rac1, calcineurin, and PKC, the specific cascade triggered by Wnt5a in hepatic stem/progenitor cells is unknown. To address this question, we analyzed the effects of specific

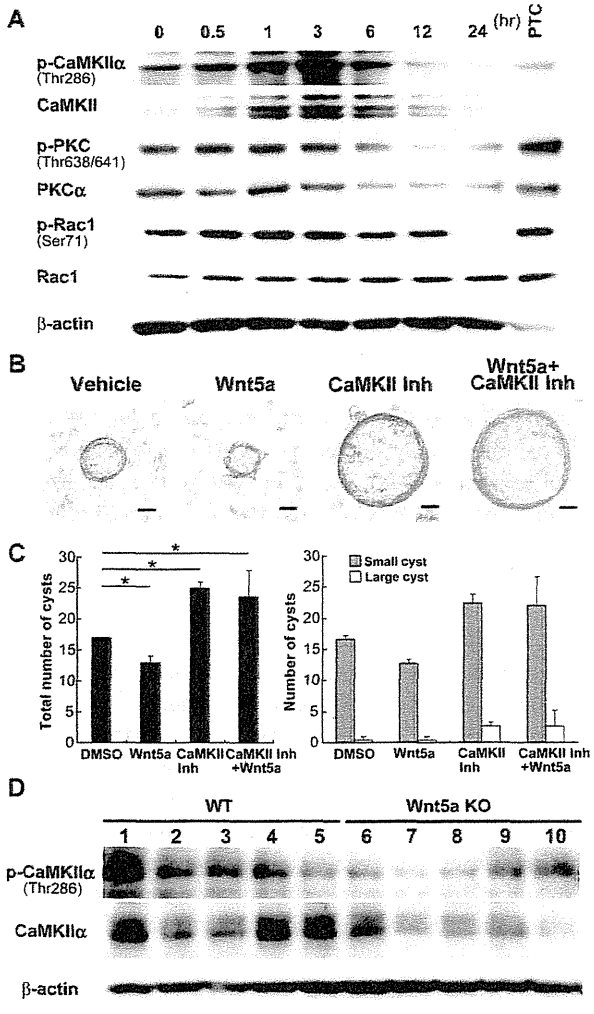

Fig. 6. Phosphorylation of CaMKII is regulated by Wnt5a stimulation in fetal liver. (A) Immunoblot analysis of p-CaMKII, p-PKC, and p-Rac1 in HPPL at pretreatment (0), and then 0.5, 1, 3, 6, 12, and 24 hours after stimulation by Wnt5a. Homogenate of whole E14.5 embryo served as a positive control (PTC). Wnt5a treatment increased the levels of both total CaMKII and p-CaMKII in HPPL, but did not change the levels of p-PKC and p-Rac1. (B) Representative phase-contrast images of cysts derived from HPPL supplemented either with vehicle (DMSO), 100 ng/mL Wnt5a, CaMKII inhibitor (KN62), or 100 ng/mL Wnt5a plus CaMKII inhibitor. Scale bars: 100 μm. (C) Numbers of bile duct-like cysts derived from HPPL in five random fields per well in cultures supplemented with vehicle (DMSO), Wnt5a, CaMKII inhibitor (KN62), or Wnt5a plus CaMKII inhibitor. The effect of Wnt5a on HPPL cysts was cancelled by KN62 treatment. $^*P < 0.05$. (D) Immunoblot analysis of p-CaMKII in E16.5 WT and Wnt5a KO livers demonstrating a decrease in p-CaMKII level in Wnt5a KO livers. Mice 1-5 and mice 6-10 are E16.5 WT and Wnt5a KOs, respectively. Results are represented as mean ± SD of three individual experiments.

inhibitors of these candidate molecules in HPPL-derived cysts, where Wnt5a is expressed (Supporting Fig. 7A). Relative to controls, inhibitors specific to CaMKII (KN93 and KN62) resulted in a significant increase in numbers of both small and large bile duct–like cysts derived from HPPL (Figs. 5A and B). In contrast, other inhibitors, including Y-27632 (Rho-kinase inhibitor), NSC23766 (Rac1 inhibitor), cyclosporin A (calcineurin inhibitor), and Go6976 (PKC inhibitor), had no effect on the number or size of HPPL-derived cysts (Fig. 5C). We examined the expression of biliary markers in HPPL-derived cysts treated with CaMKII inhibitor (KN62). Expression of MRP3, a key primary active transporter in biliary cells, in HPPL-derived cysts increased significantly with supplemental CaMKII inhibitor (Fig. 5D). There were no significant differences in mRNA levels of ALB, HNF4α, and β-catenin–related molecules between HPPL-derived cysts treated with CaMKII inhibitor and those treated with vehicle (Supporting Fig. 8). The protein level of AFP in HPPL-derived cysts treated with CaMKII inhibitor was lower than that in vehicle-supplemented controls, whereas the levels of CK19 and PCNA did not change (Fig. 5E). These data indicate that CaMKII activity suppresses the formation of HPPL-derived cysts, whereas activities of other Wnt5a-mediated candidates did not influence the efficacy of cyst formation.

Phosphorylation of CaMKII in Primary Hepatoblasts. To investigate the activation state of CaMKII in fetal and neonatal WT livers, we used immunoblots of liver homogenates derived from E14.5, E16.5, and E18.5 and postnatal day (P) 1, P7, and P14 mice to measure CaMKII phosphorylation levels.

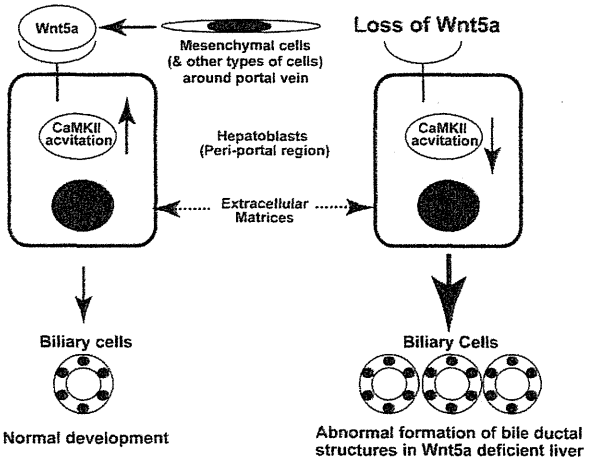

Fig. 7. Schema for the biliary differentiation of hepatoblasts in Wnt5a KO liver. Wnt5a is expressed in mesenchymal cells and other types of cells in midgestational fetal liver, and increases the level of CaMKII activation in hepatoblasts. The microenvironment around the portal vein, which consists of mesenchymal cells, other types of cells, and extracellular matrices, regulates appropriate differentiation of hepatoblasts into biliary cells, whereas loss of Wnt5a in such microenvironment leads to down-regulation of CaMKII activation in hepatoblasts and abnormally increased formation of bile ducts.

Phosphorylation at threonine-286, specifically, has been reported to maintain CaMKII in an active state.[25] Phosphorylation of PKC, a kinase that did not affect cyst formation in HPPL cells, was also examined. Whereas we detected both phosphorylated CaMKII (p-CaMKII) and PKC (p-PKC) in each fetal and neonatal liver homogenate, levels of phosphorylated CaMKII increased gradually over time (Supporting Fig. 9A, top panel), similar to the pattern of Wnt5a expression during liver development (Fig. 1A). In contrast, developmental changes in the steady-state levels and phosphorylation of PKC in these samples (Supporting Fig. 9A, lower panels) did not correspond to Wnt5a expression patterns.

Using immunostaining of FACS-purified primary hepatoblasts with anti p-CaMKII Ab, we detected p-CaMKII in >90% of FACS-purified primary hepatoblasts (Supporting Fig. 9B, upper panels); p-PKC was also detected with anti p-PKC antibodies in these cells (Supporting Fig. 9B, lower panels). These data demonstrate that both CaMKII and PKC are in an active state in primary hepatoblasts.

Wnt5a Regulates the Phosphorylation of CaMKII in Fetal Liver. To verify whether CaMKII activation is controlled by Wnt5a, levels of p-CaMKII in HPPL grown in the absence or presence of Wnt5a were examined. Immunoblot analysis revealed that Wnt5a stimulation increased the level of phosphorylated CaMKII, with p-CaMKII levels peaking 3 hours after Wnt5a supplementation and then decreasing to baseline levels after 12 hours (Fig. 6A and Supporting Fig. 10A). Similar to a previous report,[15] total CaMKII protein levels in HPPL also increased after CaMKII activation. Ratios of p-CaMKII/CaMKII also increased, peaking 3 hours after Wnt5a supplementation (Supporting Fig. 10B). In contrast, Wnt5a had no effect on p-PKC and p-Rac1 levels in HPPL (Supporting Figs. 10C and D) nor on nuclear translocation of NFAT (representative downstream molecule of calcineurin; data not shown).

We also tested the combined effect of Wnt5a plus a CaMKII inhibitor (KN62) on cyst formation in HPPL-derived cells. The number and size of cysts in HPPL-derived cells decreased with Wnt5a alone, and increased with CaMKII inhibitor alone. When used in combination (HPPL treated with both CaMKII inhibitor plus Wnt5a), the number and size of cysts was similar to CaMKII inhibitor alone, and significantly higher than cells treated with Wnt5a alone (Figs. 6B and C).

We also used immunoblots to compare p-CaMKII levels in WT and Wnt5a KO fetal liver homogenates. Levels of p-CaMKII were significantly lower in Wnt5a KO relative to WT fetal livers (Fig. 6D); quantification using densitometry revealed that p-CaMKII levels in Wnt5a KO livers were also significantly lower than those in littermate WT livers (Supporting Fig. 10E), indicating that Wnt5a mediates an increase in CaMKII phosphorylation in fetal liver.

Discussion

This study provides the first evidence of a physiological role for Wnt5a in liver development, in that Wnt5a was observed to suppress the formation of bile ducts derived from hepatoblasts. Our data showed increased expression of Sox9, Notch1, Notch2, and Jagged1 in Wnt5a KO livers (Fig. 2B and Supporting Fig. 3A), as well as abnormally increased formation of primitive ductal structures (Figs. 2E and F). In Wnt5a KO livers, the numbers of $HNF1\beta^{+}HNF4\alpha^{-}$ biliary precursor cells and primitive ductal structures were increased around the portal vein only (zone 1), whereas such cells were not observed in zone 2 or 3 (Figs. 2D-F). At E14.5, $HNF1\beta^{+}HNF4\alpha^{-}$ biliary precursor cells were not detected in Wnt5a KO livers similar to WT livers (Supporting Fig. 11A). These results suggested that lineage commitment of hepatoblasts into biliary cells is determined by the microenvironment around the portal vein, depending on the presence or absence of Wnt5a protein. The lungs and intestine of systemic Wnt5a KO mice were abnormal, while tissue structures of the pancreas and kidneys were almost normal (Supporting Fig. 12). Immunostaining analysis showed that $p75NTR^{+}$ cells were detected in E18.5 Wnt5a KO livers, similar to WT livers (Supporting Fig. 11B). These results implied that development of mesenchymal cells in E18.5 Wnt5a KO livers is not impaired compared with that in littermate WT livers. Wnt5a expression was significantly higher in mesenchymal cells than in hepatoblasts or other types of cells in midgestational WT fetal liver (Fig. 1B). Thus, the microenvironment around the portal vein, which consists of mesenchymal cells, other types of cells, and extracellular matrices, regulates appropriate cell fate decision of hepatoblasts, whereas loss of Wnt5a in such developmental niche leads to abnormally increased formation of primitive ductal structures (Fig. 7). Further investigation of this hypothesis will require conditional deletion of Wnt5a-downstream molecules in hepatoblasts at late gestational fetal stages.

Maturation of hepatoblasts to a hepatocyte lineage is regulated by several factors, including oncostatin M, HGF, and extracellular matrices.[24] Our data showed that hepatic maturation of primary hepatic stem/progenitor cells was promoted in cultures supplemented with Wnt5a (Figs. 4A and B). On the other hand, no

significant changes in hepatocyte marker expression were detected in Wnt5a KO relative to WT livers. It may be that there is functional redundancy among different Wnt family ligands *in vivo*, since several noncanonical-signaling Wnt ligands (Wnt4, Wnt5a, and Wnt11) are expressed in normal fetal liver.[26] In support of the hypothesis that other noncanonical Wnt ligands may compensate for Wnt5a, Supporting Fig. 13A shows that Wnt4 expression levels in liver increase significantly in Wnt5a KO versus WT littermates. These data strongly support our hypothesis that the effect of Wnt5a on hepatic maturation is compensated by other noncanonical Wnt ligands, such as Wnt4.

CaMKII, a serine/threonine protein kinase present in essentially every tissue, regulates important functions including modulation of ion channel activity, cellular transport, and cell morphology in neural tissues.[27] A Wnt5a-CaMKII pathway has been reported to induce osteoblastogenesis by attenuating adipogenesis in mesenchymal bone marrow stem cells.[15] Our results show that in liver, inhibition of CaMKII activity promoted bile duct–like cyst formation (Figs. 5A and B), and that phosphorylation of CaMKII is dependent on Wnt5a stimulation (Fig. 6). Although these results provide strong support for our hypothesis that Wnt5a stimulates CaMKII in hepatoblasts, we have not identified which molecules function downstream of CaMKII.

CaMKII has been reported to activate the transforming growth factor β–activated kinase 1 (TAK1)-Nemo-like kinase (NLK) pathway, and that resulting phosphorylation of T cell factor inhibits β-catenin–dependent transcription.[28] On the other hand, CaMKII-TAK1-NLK signaling induces bone marrow mesenchymal stem cells to undergo osteoblastogenesis depending on specific downstream signaling cascades.[15] Our expression analysis showed that expression levels of *Cyclin D1* and *c-Myc* (the direct target molecules of β-catenin activation) did not change in Wnt5a KO mice *in vivo* (Supporting Fig. 4) nor in HPPL-derived cysts treated with CaMKII inhibitor *in vitro* (Supporting Fig. 8), compared with the respective control samples. Preliminary data (not shown) demonstrated that the levels of TAK1 mRNA and protein during development did not correlate with those of Wnt5a and p-CaMKII in whole liver lysates. Moreover, Wnt5a stimulation did not increase the level of activated β-catenin in HPPL (Supporting Figs. 13B and C). These results suggest that the Wnt5a-CaMKII pathway does not activate β-catenin in hepatoblasts. On the other hand, Wnt5a stimulation increased the level of stabilized p53 (phosphorylated at Ser15) in HPPL (Supporting Figs. 13B and D), suggesting that stabilization of p53 is associated with Wnt5a-CaMKII signaling. Further study will be needed to clarify this issue.

Recent studies have shown pathological roles for Wnt5a in various organs; addition of recombinant Wnt5a significantly reduced the migratory capacity of colorectal cancer cell line.[29] Whereas increased Wnt5a expression correlates with advanced stages of gastric cancer with poor prognosis,[30] there is no definitive data about Wnt5a in the progression of hepatocellular carcinomas. In this study, we reveal one function of Wnt5a in fetal liver in the suppression the biliary differentiation of hepatic stem/progenitor cells. To clarify the pathological role of Wnt5a in liver disease, inducible systemic Wnt5a KO mice or liver-specific CaMKII KO mice would be needed in future studies. Any future evidence demonstrating a role for Wnt5a in adult hepatic stem/progenitor cells and cancer stem cells may lead to studies of Wnt5a signaling as a therapeutic target against abnormal bile ductal formation in the liver or cholangiocellular carcinoma.

Acknowledgment: We thank Prof. A. Miyajima (the University of Tokyo) for the gift of anti-CK19 antibody. We thank K. Itoh, K. Okada, and A. Yanagida (Institute of Medical Science, the University of Tokyo) for excellent technical assistance.

References

1. Turner R, Lozoya O, Wang Y, Cardinale V, Gaudio E, Alpini G, et al. Human hepatic stem cell and maturational liver lineage biology. HEPATOLOGY 2011;53:1035-1045.
2. Cardinale V, Wang Y, Carpino G, Cui CB, Gatto M, Rossi M, et al. Multipotent stem/progenitor cells in human biliary tree give rise to hepatocytes, cholangiocytes, and pancreatic islets. HEPATOLOGY 2011;54:2159-2172.
3. Kubota H, Reid LM. Clonogenic hepatoblasts, common precursors for hepatocytic and biliary lineages, are lacking classical major histocompatibility complex class I antigen. Proc Natl Acad Sci USA 2000;97:12132-12137.
4. Kakinuma S, Ohta H, Kamiya A, Yamazaki Y, Oikawa T, Okada K, et al. Analyses of cell surface molecules on hepatic stem/progenitor cells in mouse fetal liver. J Hepatol 2009;51:127-138.
5. Zhou H, Rogler LE, Teperman L, Morgan G, Rogler CE. Identification of hepatocytic and bile ductular cell lineages and candidate stem cells in bipolar ductular reactions in cirrhotic human liver. HEPATOLOGY 2007;45:716-724.
6. Oikawa T, Kamiya A, Kakinuma S, Zeniya M, Nishinakamura R, Tajiri H, et al. Sall4 regulates cell fate decision in fetal hepatic stem/progenitor cells. Gastroenterology 2009;136:1000-1011.
7. Suzuki A, Sekiya S, Buscher D, Belmonte JCI, Taniguchi H. Tbx3 controls the fate of hepatic progenitor cells in liver development by suppressing p19(ARF) expression. Development 2008;135:1589-1595.
8. van Amerongen R, Nusse R. Towards an integrated view of Wnt signaling in development. Development 2009;136:3205-3214.
9. Kikuchi A, Yamamoto H, Sato A, Matsumoto S. Wnt5a: its signalling, functions and implication in diseases. Acta Physiol (Oxf) 2012;204:17-33.

10. Tan XP, Yuan YZ, Zeng G, Apte U, Thompson MD, Cieply B, et al. beta-catenin deletion in hepatoblasts disrupts hepatic morphogenesis and survival during mouse development. HEPATOLOGY 2008;47: 1667-1679.
11. Yamaguchi TP, Bradley A, McMahon AP, Jones S. A Wnt5a pathway underlies outgrowth of multiple structures in the vertebrate embryo. Development 1999;126:1211-1223.
12. Li CG, Xiao J, Hormi K, Borok Z, Minoo P. Wnt5a participates in distal lung morphogenesis. Dev Biol 2002;248:68-81.
13. Cervantes S, Yamaguchi TP, Hebrok M. Wnt5a is essential for intestinal elongation in mice. Dev Biol 2009;326:285-294.
14. Nemeth MJ, Topol L, Anderson SM, Yang YZ, Bodine DM. Wnt5a inhibits canonical Wnt signaling in hematopoietic stem cells and enhances repopulation. Proc Natl Acad Sci USA 2007;104: 15436-15441.
15. Takada I, Mihara M, Suzawa M, Ohtake F, Kobayashi S, Igarashi M, et al. A histone lysine methyltransferase activated by non-canonical Wnt signalling suppresses PPAR-gamma transactivation. Nat Cell Biol 2007;9:1273-1285.
16. Parish CL, Castelo-Branco G, Rawal N, Tonnesen J, Sorensen AT, Salto C, et al. Wnt5a-treated midbrain neural stem cells improve dopamine cell replacement therapy in parkinsonian mice. J Clin Invest 2008;118:149-160.
17. Zeng G, Awan F, Otruba W, Muller P, Apte U, Tan XP, et al. Wnt'er in liver: expression of Wnt and frizzled genes in mouse. HEPATOLOGY 2007;45:195-204.
18. Tanimizu N, Saito H, Mostov K, Miyajima A. Long-term culture of hepatic progenitors derived from mouse Dlk+ hepatoblasts. J Cell Sci 2004;117:6425-6434.
19. Tanimizu N, Miyajima A, Mostov KE. Liver progenitor cells develop cholangiocyte-type epithelial polarity in three-dimensional culture. Mol Biol Cell 2007;18:1472-1479.
20. Antoniou A, Raynaud P, Cordi S, Zong Y, Tronche F, Stanger BZ, et al. Intrahepatic bile ducts develop according to a new mode of tubulogenesis regulated by the transcription factor SOX9. Gastroenterology 2009;136:2325-2333.
21. Lozier J, McCright B, Gridley T. Notch signaling regulates bile duct morphogenesis in mice. PLoS One 2008;3:e1851.
22. Tchorz JS, Kinter J, Muller M, Tornillo L, Heim MH, Bettler B. Notch2 signaling promotes biliary epithelial cell fate specification and tubulogenesis during bile duct development in mice. HEPATOLOGY 2009;50:871-879.
23. Si-Tayeb K, Lemaigre FP, Duncan SA. Organogenesis and development of the liver. Dev Cell 2010;18:175-189.
24. Kamiya A, Kojima N, Kinoshita T, Sakai Y, Miyaijma A. Maturation of fetal hepatocytes in vitro by extracellular matrices and oncostatin M: induction of tryptophan oxygenase. HEPATOLOGY 2002;35:1351-1359.
25. Patton BL, Molloy SS, Kennedy MB. Autophosphorylation of type II CaM kinase in hippocampal neurons: localization of phospho- and dephosphokinase with complementary phosphorylation site-specific antibodies. Mol Biol Cell 1993;4:159-172.
26. Konishi S, Yasuchika K, Ishii T, Fukumitsu K, Kamo N, Fujita N, et al. A transmembrane glycoprotein, gp38, is a novel marker for immature hepatic progenitor cells in fetal mouse livers. In Vitro Cell Dev Biol Anim 2011;47:45-53.
27. Yamauchi T. Neuronal Ca2+/calmodulin-dependent protein kinase II—discovery, progress in a quarter of a century, and perspective: implication for learning and memory. Biol Pharm Bull 2005;28:1342-1354.
28. Ishitani T, Kishida S, Hyodo-Miura J, Ueno N, Yasuda J, Waterman M, et al. The TAK1-NLK mitogen-activated protein kinase cascade functions in the Wnt-5a/Ca2+ pathway to antagonize Wnt/beta-catenin signaling. Mol Cell Biol 2003;23:131-139.
29. Dejmek J, Dejmek A, Safholm A, Sjolander A, Andersson T. Wnt-5a protein expression in primary dukes B colon cancers identifies a subgroup of patients with good prognosis. Cancer Res 2005;65: 9142-9146.
30. Kurayoshi M, Oue N, Yamamoto H, Kishida M, Inoue A, Asahara T, et al. Expression of Wnt-5a is correlated with aggressiveness of gastric cancer by stimulating cell migration and invasion. Cancer Res 2006;66: 10439-10448.

Journal of Gastroenterology and Hepatology

JGHF

doi:10.1111/jgh.12138

EDITORIALS

NX-PVKA assay, a conventional but refined prognostic biomarker for hepatocellular carcinoma

Naoya Sakamoto

Department of Gastroenterology and Hepatology, Hokkaido University, Hokkaido, Japan

See article in *J. Gastroenterol. Hepatol.* 2013; 28: 671–677.

Hepatocellular carcinoma (HCC) is one of the most common neoplasms worldwide. The recent dramatic increase of HCC cases is associated with chronic hepatitis B and C.[1] Worldwide, there are 300 million people infected with hepatitis B virus and 170 million with hepatitis C virus, respectively.

Prothrombin, a 72-kDa plasma protein, is synthesized in hepatocytes as a precursor with 10 glutamic acid (Glu) residues. Under physiological condition, these Glu residues are converted into gamma-carboxy glutamic acid (Gla) by gamma-glutamylcarboxylase, which uses vitamin K as a cofactor. However, when gamma-glutamylcarboxylation is impaired, Glu residues of prothrombin remain unconverted, and a des-carboxy prothrombin (DCP) is released into the bloodstream as a result. DCP is elevated in many patients with HCC, as well as those with vitamin K deficiency, so that raised plasma DCP can result from the administration of vitamin K antagonists like warfarin or impaired uptake of vitamin K in cholestasis with hyperbilirubinemia.

Plasma level lf DCP is significantly elevated in patients with HCC, and is a clinically established HCC marker. For small tumors, measurement of both alpha fetoprotein (AFP) and DCP is recommended, because DCP is more specific for HCC than AFP.

DCP is potentially valuable primarily as a prognostic biomarker, which would be predictive of rapid tumor progression and provide information about a possible poor prognosis.[2] This is because DCP-positive HCCs show aggressive and invasive distinctiveness. A high DCP level implies a poor prognosis, and a slight increase in the DCP concentration after therapy could suggest recurrence.[2] Kiriyama *et al.* demonstrated significantly poorer prognosis in "triple-positive" HCC patients, who were positive for all three available serum HCC markers, AFP, AFP-L3, and DCP.[3] Besides its significance in serum HCC marker, DCP acts as an autologous mitogen for HCC cell lines. *In vitro*, DCP stimulates cell proliferation in HCC lines through the activation of cMET-Jak1 signal transducer and an activator of the transcription 3 signaling pathway.[4] Moreover, DCP can induce both cell proliferation and migration of human umbilical vein endothelial cells. DCP has several variants based on the number of Glu residues. It is reported that there are differences in the number of Glu residues in DCP between patients with HCC and those taking warfarin.[5,6] The conventional DCP assay, which uses the MU-3 antibody, detects DCP with 9–10 Glu residues and has lower affinity for DCP with one to five Glu residues. Toyoda *et al.* have reported a new DCP assay which specifically detects DCP with fewer Glu residues by using P-11 and P-16 monoclonal antibodies (Fig. 1). They have demonstrated the usefulness of this new test as an HCC marker in patients who were taking warfarin.[7]

In this issue of the *Journal of Gastroenterology and Hepatology*, Takeji *et al.* have reported an assay to detect DCP variants with fewer Glu residues, named NX-PVKA assay in HCC patients.[8] They included 197 HCC patients and measured NX-PVKA and the NX-PVKA ratio (DCP/NX-PVKA-R), along with conventional DCP, AFP, and AFP-L3 prior to HCC treatment. They demonstrated that NX-PVKA was the strongest independent prognostic marker for overall survival with a hazard ratio of 81.32 by multivariate analysis. NX-PVKA level of greater than 100 mAU/mL correlated with significantly lower survival rates. NX-PVKA level was also significantly associated with platelet count, prothrombin time, C-reactive protein (CRP), sex, maximum tumor size, number of nodules, and portal venous invasion by HCC. With the said results, they established a prognostic model by using parameters; sex, serum albumin, 2 gamma glutamyl transferase, leucin aminopeptidase, CRP, hyaluronic acid, and NX-PVKA. Overall, they have presented a novel PVKA assay that associates with HCC prognosis more precisely than the conventional assays.

The authors acknowledge several shortcomings in the present study. Because this is a retrospective study of patients from a single center in Japan, the results, including the prognostic model, should be validated using an independent testing cohort of patients. In addition, the patients enrolled in this study had several etiologies of liver damage and received different treatments. Overall survival is determined by patient and tumor factors, liver cirrhosis and functional reserve, and by the treatment modality. Because treatment was not considered, its influence on the overall survival remains unclear. Additional large-scale and multicenter studies are warranted to verify their results. Nonetheless, the combination of NX-DCP and a conventional DCP assay is useful to identify HCC in patients taking the vitamin K antagonist warfarin. Moreover, NX-PVKA, along with their proposed prognostic model, potentially offers an efficient tool to predict long- and short-term prognosis and overall survival of HCC patients.

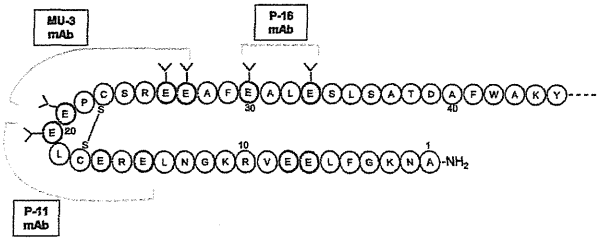

Figure 1 γ-carboxylation of glutamic acid residues in prothombin. The illustration shows amino acid sequence of N-terminus prothrombin (GLA domain). Immunological epitopes for three monoclonal antibodies (mAb), MU-3, P-11, and P-16 mAbs, are shown. MU-3 is for conventional assay, and P-11 and P-16 are for NX-PVKA assay, respectively. Ⓔ, glutamic acid; Ⓨ, γ-carboxy glutamic acid.

Accepted for publication 21 January 2013.

Correspondence
Professor Naoya Sakamoto, Department of Gastroenterology and Hepatology, Hokkaido University, North 15, West 7, Kita-ku, Sapporo, Hokkaido 060-8638, Japan. Email: sakamoto@med.hokudai.ac.jp

References

1 El-Serag HB. Translational research: the study of community effectiveness in digestive and liver disorders. *Gastroenterology* 2007; **132**: 8–10.
2 Suehiro T, Sugimachi K, Matsumata T, Itasaka H, Taketomi A, Maeda T. Protein induced by vitamin K absence or antagonist II as a prognostic marker in hepatocellular carcinoma. Comparison with alpha-fetoprotein. *Cancer* 1994; **73**: 2464–71.
3 Kiriyama S, Uchiyama K, Ueno M *et al.* Triple positive tumor markers for hepatocellular carcinoma are useful predictors of poor survival. *Ann. Surg.* 2011; **254**: 984–91.
4 Suzuki M, Shiraha H, Fujikawa T *et al.* Des-gamma-carboxy prothrombin is a potential autologous growth factor for hepatocellular carcinoma. *J. Biol. Chem.* 2005; **280**: 6409–15.
5 Liebman HA. Isolation and characterization of a hepatoma-associated abnormal (des-gamma-carboxy)prothrombin. *Cancer Res.* 1989; **49**: 6493–7.
6 Uehara S, Gotoh K, Handa H, Tomita H, Senshuu M. Distribution of the heterogeneity of des-gamma-carboxyprothrombin in patients with hepatocellular carcinoma. *J. Gastroenterol. Hepatol.* 2005; **20**: 1545–52.
7 Toyoda H, Kumada T, Osaki Y, Tada T, Kaneoka Y, Maeda A. Novel method to measure serum levels of des-gamma-carboxy prothrombin for hepatocellular carcinoma in patients taking warfarin: a preliminary report. *Cancer Sci.* 2012; **103**: 921–5.
8 Takeji S, Hirooka M, Koizumi Y *et al.* Des-gamma-carboxy prothrombin identified by P-11 and P-16 antibodies reflects prognosis for patients with hepatocellular carcinoma. *J. Gastroenterol. Hepatol.* 2013; **28**: 671–7.

Heme oxygenase-1 and platelets in hepatic ischemia reperfusion injury

Benjamin L Woolbright and Hartmut Jaeschke

Department of Pharmacology, Toxicology and Therapeutics, University of Kansas Medical Center, Kansas City, Kansas, USA

See article in *J. Gastroenterol. Hepatol.* 2013; 28: 700–706.

Ischemia reperfusion injury (IRI) in the liver is a challenge clinically in cases of both warm (tumor resection surgery) and cold ischemia (liver transplantation). During IRI, hepatocytes are exposed to prolonged periods of ischemia, which predispose the cells toward injury during reperfusion. When the tissue is reperfused, the resident macrophages of the liver (Kupffer cells) and newly recruited neutrophils produce reactive oxygen species (ROS) in response to damage signals released from injured hepatocytes, resulting in extensive hepatic necrosis.[1,2] Traditional preconditioning, where the liver is exposed to brief, cyclic periods of ischemia and reperfusion, protects the liver against IRI via the induction of multiple genes which help to detoxify ROS.[1] Among these genes are multiple targets of the transcription factor Nrf2, a master regulator of the oxidant stress response.[2] Selective overexpression or induction of many of these target genes, including heme oxygenase-1 (HO-1), is protective against IRI through mechanisms that have been studied extensively, but are not fully elucidated.[3] HO-1 is thought to enhance the antioxidant capacity of cells directly by formation of the antioxidants bilirubin and biliverdin, while additional products of HO-1 activity such as carbon monoxide (CO) may function as a vasodilator, improving blood flow to the postischemic tissue.[4] HO-1 induction also partially mediates protection from IRI by a number of other molecules including the sphingosine receptor agonist FTY720, volatile anesthetics such as isoflurane and the cytoprotective effects of anti-inflammatory cytokines such as IL-13.[5]

Inactivation of Kupffer cells has previously been shown to be protective against IRI via reduction of ROS formation by these macrophages during reperfusion.[6] Complement activation initiated by the release of cell contents during the early reperfusion phase was shown to trigger the Kupffer cell-induced oxidant stress.[7] Tamura and colleagues reported previously that more than 50% of adhering platelets in sinusoids were associated with Kupffer cells during the early reperfusion period and that an anti-platelet antiserum attenuated Kupffer cell-mediated early reperfusion injury implying that platelets may contribute to Kupffer cell activation.[8] In the current issue of the *Journal of Gastroenterology and Hepatology*, the authors expanded these findings by demonstrating that induction of HO-1 by cobalt protoporphyrin (CoPP) reduced platelet adherence to sinusoidal endothelial cells and to Kupffer cells and almost completely prevented reperfusion injury during the first 2 h.[9] Although the authors did not investigate the mechanisms of protection in detail, it is likely that strengthening of the endogenous antioxidant defense in hepatocytes and in the sinusoidal lining cells by HO-1 induction led to enhanced resistance against endogenous (damaged mitochondria during ischemia) and exogenous sources (Kupffer cells) of oxidant stress, which effectively attenuated the initiation of an inflammatory response, platelet activation, and injury during the early reperfusion phase. The study by Tamura *et al.*[9] also confirms an important concept. By strengthening the endogenous antioxidant defense mechanisms against ROS-mediated cell death, CoPP treatment attenuates the early cell death and prevents the amplification of the injury by an inflammatory response and is thus more effective and clinically relevant than an intervention that targets selectively inflammatory cells. In addition, by not directly inactivating inflammatory cells, the vital host defense function of these leukocytes is not impaired.

The role of platelets during IRI remains controversial. Early studies looking at models of reduced platelet adhesion using mice deficient in adhesion molecules such as P-selectin showed a reduction in early reperfusion injury and enhanced survival after 90 min of ischemia.[10] However, these beneficial effects of reduced platelet adhesion were likely mediated by a concurrent reduction in neutrophil recruitment and thus a reduction of the neutrophil-mediated oxidant stress and cell killing, which is a critical determinant of reperfusion injury.[1] A later report implicated that platelet adhesion in sinusoids increases microcirculatory perfusion failure, which correlates with enhanced reperfusion injury.[11] Furthermore, Tamura *et al.* suggested that adhesion of platelets to Kupffer cells promotes their activation during reperfusion.[9] However, a more recent study

Accepted for publication 2 January 2013.

Correspondence
Hartmut Jaeschke, Department of Pharmacology, Toxicology and Therapeutics, University of Kansas Medical Center, 3901 Rainbow Bvd, MS 1018, Kansas City, KS 66160, USA. Email: hjaeschke@kumc.edu

JVI
Journals.ASM.org

Hepatitis C Virus Replication Is Modulated by the Interaction of Nonstructural Protein NS5B and Fatty Acid Synthase

Jing-Tang Huang,[a,b] Ching-Ping Tseng,[c] Mei-Huei Liao,[a] Shao-Chun Lu,[d] Wei-Zhou Yeh,[a] Naoya Sakamoto,[e] Chuan-Mu Chen,[b] Ju-Chien Cheng[a]

Department of Medical Laboratory Science and Biotechnology, China Medical University, Taichung, Taiwan[a]; Department of Life Sciences, National Chung Hsing University, Taichung, Taiwan[b]; Department of Medical Biotechnology and Laboratory Science, Chang Gung University, Taoyuan, Taiwan[c]; Graduate Institute of Biochemistry and Molecular Biology, National Taiwan University, Taipei, Taiwan[d]; Department of Gastroenterology and Hepatology, Tokyo Medical and Dental University, Tokyo, Japan[e]

Hepatitis C virus (HCV) nonstructural protein 5B (NS5B) is an RNA-dependent RNA polymerase (RdRp) that acts as a key player in the HCV replication complex. Understanding the interplay between the viral and cellular components of the HCV replication complex could provide new insight for prevention of the progression of HCV-associated hepatocellular carcinoma (HCC). In this study, the NS5B protein was used as the bait in a pulldown assay to screen for NS5B-interacting proteins that are present in Huh7 hepatoma cell lysates. After mass spectrophotometric analysis, fatty acid synthase (FASN) was found to interact with NS5B. Coimmunoprecipitation and double staining assays further confirmed the direct binding between NS5B and FASN. The domain of NS5B that interacts with FASN was also determined. Moreover, FASN was associated with detergent-resistant lipid rafts and colocalized with NS5B in active HCV replication complexes. In addition, overexpression of FASN enhanced HCV expression in Huh7/Rep-Feo cells, while transfection of FASN small interfering RNA (siRNA) or treatment with FASN-specific inhibitors decreased HCV replication and viral production. Notably, FASN directly increased HCV NS5B RdRp activity *in vitro*. These results together indicate that FASN interacts with NS5B and modulates HCV replication through a direct increase of NS5B RdRp activity. FASN may thereby serve as a target for the treatment of HCV infection and the prevention of HCV-associated HCC progression.

Hepatitis C virus (HCV) is a positive-stranded RNA virus classified in the *Hepacivirus* genus in the family *Flaviviridae*. The 9.6-kb viral RNA genome encodes a precursor polyprotein that is processed to generate at least 10 viral proteins, including structural proteins (core, E1, E2, and p7) and nonstructural proteins (NS2, NS3, NS4A, NS4B, NS5A, and NS5B) (1). The NS5B RNA polymerase, together with other nonstructural viral proteins (NS3, NS4A, NS4B, and NS5A) and host factors, constitutes the active replication complexes (RC) for viral RNA replication. These proteins are directly or indirectly associated with the endoplasmic reticulum (ER)-derived structure called the "membranous web," where replication occurs (2, 3). However, the exact host factors and detailed interactions within the RC remain to be determined.

HCV infection usually causes chronic hepatitis and frequently leads to cirrhosis and hepatocellular carcinoma (HCC). Besides, HCV-induced end-stage liver disease is an important indication for liver transplantation in most of the Western countries (4, 5). At present, no effective vaccine to prevent HCV infection is available. The current treatment strategies for HCV infection are valid only for individuals with a particular single nucleotide polymorphism (SNP) in the interleukin-28B gene or for infections caused by certain viral genotypes (6). Accordingly, the prevalence of hepatic steatosis in HCV-infected patients is much higher than that in the general population or in hepatitis B virus (HBV)-infected patients (7). Hepatic steatosis has also been reported to be associated with an increased rate of HCC in chronic hepatitis C patients (8).

Lipid metabolic pathways are essential for the entry, secretion, and replication of HCV. For example, apolipoprotein E (apoE) is essential for the production of HCVcc (HCV produced in cell culture) and for viral entry (9, 10). Downregulation of apoA-I decreases levels of HCV replication and viral particle production in cell culture (11). HCV coopts the secretory pathway of very low density lipoprotein (VLDL) for its own secretion (12, 13). Moreover, HCV replication is regulated through induction of lipogenic gene expression in HCV replicon cells (14) or geranylgeranylation of host proteins required for HCV RNA replication (15, 16). Fatty acid synthesis is also required for HCV RNA replication (14). Inhibition of fatty acid synthase (FASN) by cerulenin (17) or C75 (18) reduces the replication of subgenomic HCV replicons as well as JFH-1-based HCVcc virion production. Although the underlying mechanisms are not yet completely understood, these studies imply that FASN is essential for HCV replication.

In this study, HCV NS5B was used as the bait to screen for NS5B-interacting proteins that are present in Huh7 hepatoma cell lysates. After mass spectrophotometric analysis, FASN was found to interact with NS5B, and this interaction was further confirmed *in vitro* and *in vivo*. Our data indicate that FASN interacts with NS5B to enhance NS5B RNA-dependent RNA polymerase (RdRp) activity and subsequently facilitate HCV replication. Taken together, these data suggest a critical role for FASN-NS5B

Received 15 September 2012 Accepted 7 February 2013
Published ahead of print 20 February 2013
Address correspondence to Ju-Chien Cheng, jccheng@mail.cmu.edu.tw, or Chuan-Mu Chen, chchen1@dragon.nchu.edu.tw.
Supplemental material for this article may be found at http://dx.doi.org/10.1128/JVI.02526-12.

doi:10.1128/JVI.02526-12

interaction in the modulation of HCV replication. The roles of FASN in the regulation of HCV pathogenesis are also discussed.

MATERIALS AND METHODS

Cells and materials. The HCV subgenomic replicon cell line Sg-PC2 (19) was a gift from Jing-Hsiung Ou (University of Southern California, Los Angeles, CA). The HCV subgenomic replicon cell line Huh7/Rep-Feo (genotype 1b) expressing a luciferase construct was obtained from Naoya Sakamoto (Tokyo Medical and Dental University, Tokyo, Japan). The Huh7.5.1 cells and plasmid JC1-Luc2A, which replaces the Rluc gene of pJ6/JFH(p7-Rlu2A) with the firefly luciferase (Luc) gene, were kindly provided by Robert T. Schooley (University of California, San Diego). A rabbit polyclonal antibody against the HCV NS5B protein was kindly provided by Takaji Wakita (National Institute of Infectious Diseases, Tokyo, Japan). Plasmid pCMV-SPORT6-FASN, the transfection reagent Lipofectamine 2000 (LF2000), and the Alexa Fluor 568-conjugated goat anti-rabbit IgG were purchased from Invitrogen (Carlsbad, CA). The synthetic small interfering RNA (siRNA) for FASN (siFASN; 5′-AACCCTG AGATCCCAGCGCTG-3′) and siCONTROL nontargeting siRNA-2 (siC) were from Dharmacon (Lafayette, CO). The siRNA for green fluorescent protein (siGFP) was purchased from Ambion (Austin, TX). The pLKO.1 vector carrying short hairpin RNA (shRNA) for GFP (pLKO.1-shGFP; clone identification [ID], TRCN0000072197), pLKO.1-shFASN (clone IDs, TRCN000003127 and TRCN000003128), pCMVdR, and pMD2.G were purchased from the National RNAi Core Facility (Academia Sinica, Taipei, Taiwan). The transfection reagent Arrest-In was obtained from Open Biosystems (Lafayette, CO). The FASN inhibitor C75 and the anti-caveolin-2, anti-calnexin, and mouse monoclonal anti-HCV NS5B antibodies were purchased from Enzo Life Sciences (Farmingdale, NY). S7 nuclease and the FuGENE HD transfection reagent were purchased from Roche (Mannheim, Germany). Glutathione Sepharose 4B and protein A Sepharose were purchased from GE Healthcare (Piscataway, NJ). The 3-(4,5-dimethylthiazol-2-yl)-5-(3-carboxymethoxyphenyl)-2-(4-sulfophenyl)-2H-tetrazolium (MTS) reduction assay and Bright-Glo luciferase assay reagents were purchased from Promega (Madison, WI). The anti-HCV NS5A antibody was purchased from BioDesign (Carmel, NY). The anti-HCV NS3 antibody was purchased from Novocastra (Newcastle, United Kingdom). The anti-HCV core antibody was purchased from Thermo Scientific (Rockford, IL). Proteinase K, pyruvate kinase, the anti-β-actin antibody, and the anti-Flag M2 affinity gel were purchased from Sigma (St. Louis, MO). The anti-FASN and anti-GRP78 antibodies and normal rabbit IgG were purchased from Santa Cruz Biotechnology (Santa Cruz, CA). HiLyte Fluor 488-conjugated goat anti-mouse IgG was purchased from AnaSpec (San Jose, CA). The NS5B inhibitor 2′-C-methyladenosine (2′CMA) was purchased from Carbosynth (Berkshire, United Kingdom). Phosphoenolpyruvate was purchased from Alfa Aesar (Ward Hill, MA). EasyBlocker and EasyBlot anti-rabbit IgG were purchased from GeneTex (Irvine, CA). [α-^{32}P]CTP was purchased from Perkin-Elmer (Wellesley, MA).

Plasmid construction. To generate pGEX-2T-NS5Bd21, the NS5B fragment with a deletion of the C-terminal 21 amino acids (NS5Bd21) (20) was amplified by PCR using the forward primer NS5bGF (5′-CGCGGATCCAC CATGTCCTACACATGG-3′) and the reverse primer NS5bER (5′-GGC TACTTAAGTCAGCGGGGTCGGGCACGAG-3′). The PCR product was then subcloned into the pGEM-T Easy vector (Promega, Madison) to generate pGEN-T-NS5B. The BamHI-EcoRI fragment of pGEM-T-NS5B, containing the NS5B coding sequences, was subcloned into pGEX-2T (GE Healthcare, Sweden). The NS5Bd21 fragment from pGEM-T-NS5B was further subcloned into pFlag-CMV2 to generate pCMV-Flag-NS5B or into pET32a to generate pET32a-NS5Bd21.

For NS5B deletion mutants, the deletion fragments were generated by PCR using pCMV-Flag-NS5B as the template. The primer sets are listed in Table 1. The PCR product was ligated into the pTOPO vector and was further subcloned into pFlag-CMV2 to generate pCMV-Flag-NS5B/1-180, pCMV-Flag-NS5B/1-335, and pCMV-Flag-NS5B/179-570.

TABLE 1 Primer sequences for plasmid constructs

Primer name	Primer sequence[a]	Length (mer)
CNS5BYF	5′-CACGCGTCGACGTCGATGTCCTACACATGG-3′	30
CNS5BtYR	5′-GGACTAGTCCGCGGGGTCGGGCACGAG-3′	27
NS5BGF	5′-CGCGGATCCACCATGTCCTACACATGG-3′	27
NS5BER	5′-GGCTAGAATTCTCAGCGGGGTCGGGCACGAG-3′	31
NS5B 1-180 F	5′-TTCGATGTCCTACACATGGACA-3′	22
NS5B 1-180 R	5′-TCAGGAGACCACATCGTAAAGG-3′	22
NS5B 179-570 F	5′-GCATCCCAAGCTTGTCTCCACCCTTCCTCAAG-3′	32
NS5B 179-570 R	5′-CGGAATTCTCAGCGGGGTCGGGCACGAGA-3′	29
NS5B 1-335 F	5′-CCCAAGCTTTCGATGTCCTACACATGGACAG-3′	31
NS5B 1-335 R	5′-CGGAATTCTCAGCTCGCCGCGTCCTCCTGG-3′	30

[a] Underlining indicates the SalI site for CNS5BYF, the SpeI site for CNS5BtYR, the BamHI site for NS5BGF, the EcoRI site for NS5BER, the HindIII site for NS5B 179-570 F and NS5B 1-335 F, and the EcoRI site for NS5B 179-570 R and NS5B 1-335 R.

To generate pcDNA3.1/HisC-FASN, an EcoRI-XhoI DNA fragment of pCMV-SPORT6-FASN containing FASN cDNA sequences was cloned into pCMV-Tag3 (Stratagene). Then an EcoRI-XhoI DNA fragment containing FASN sequences was subcloned into pcDNA3.1/HisC (Invitrogen) to generate pcDNA3.1/HisC-FASN.

GST pulldown assay. The glutathione *S*-transferase (GST) pulldown assay was performed as described by the manufacturer (GE Healthcare). Briefly, plasmids pGEX-2T-NS5Bd21 and pGEX-2T were transformed into the *Escherichia coli* strain BL21(DE3)pLysS, respectively. The bacteria were then induced with 1 mM isopropyl β-D-1-thiogalactopyranoside (IPTG) at 22°C overnight and were subsequently collected by centrifugation at 6,000 rpm for 20 min. Cell pellets were resuspended in lysis buffer (1× phosphate-buffered saline [PBS] containing 1% Triton X-100 and 1 mM dithiothreitol [DTT]) and were sonicated for 4 min (10-s sonication and 10-s pause). Ten milligrams of bacterial lysates was incubated with 66 μl glutathione Sepharose 4B for 1 h at 4°C. After three washes with lysis buffer, the GST- and GST fusion protein-binding beads were mixed with 1.5 mg Huh7 cell lysates suspended in GST pulldown buffer {10 mM Tris-HCl, 140 mM NaCl, 0.5 mM calcium chloride, 0.5 mM magnesium chloride, and freshly added 1% 3-[(3-cholamidopropyl)-dimethylammonio]-1-propanesulfonate (CHAPS)} at 4°C overnight. The beads were then washed four times with GST pulldown buffer and were separated by 10% sodium dodecyl sulfate-polyacrylamide gel electrophoresis (SDS-PAGE) for further analyses.

Silver staining. After protein separation by SDS-PAGE, the polyacrylamide gel was fixed in buffer A (50% methanol and 25% acetic acid) for 2 h, followed by incubation with buffer B (30% methanol) for 15 min. After three rinses in distilled water, the gel was incubated in buffer C (0.8 mM sodium thiosulfate) for 2 min and was rinsed three times in distilled water. The gel was then incubated with buffer D (0.2% silver nitrate) for 25 min and was rinsed twice with distilled water. The gel was subsequently developed with buffer E (0.28 M sodium carbonate, 0.85% formaldehyde, and 16 μM sodium thiosulfate) until protein bands were visible. The reaction was stopped by rinsing the gel briefly in distilled water, and the gel was then incubated in buffer F (42 mM EDTA).

In-gel digestion and MALDI-TOF mass spectrometric analysis. The band of interest displayed by silver staining was subjected to excision. Gel digestion was performed as described previously (21). Briefly, the gel was washed with wash buffer (25 mM NH_4HCO_3 and 50% acetonitrile [ACN]) and was destained in a solution with 1% potassium ferricyanide and 1.5% sodium thiosulfate. The protein was reduced in 10 mM dithiothreitol in 25 mM NH_4HCO_3 for 1 h at 56°C and was alkylated with 55 mM iodoacetamide in 25 mM NH_4HCO_3 at room temperature for 30 min in the dark. The protein was dehydrated with ACN and was then digested with trypsin at 37°C overnight, followed by extraction with 0.5% trichloroacetic acid (TCA). Matrix-assisted laser desorption ionization–time of flight mass spectrometric (MALDI-TOF MS) analysis was then performed using the Ultraflex MALDI-TOF mass spectrometer (Bruker-Daltonics).

The peptide sequence data were searched against the MASCOT search database (Matrix Science, London, United Kingdom).

Transfection. HEK293T or Huh7 cells were seeded into 60-mm or 35-mm culture dishes for 24 h. Three micrograms of pCMV3B-FASN and 3 μg of pCMV-Flag-NS5B or pcDNA-NS5A were cotransfected into 293T cells by use of the Arrest-In transfection reagent (Thermo Scientific) or into Huh7 cells by use of the Fugene HD transfection reagent (Roche). At 48 h posttransfection, either cell lysates were prepared for immunoprecipitation or the cells were fixed for immunofluorescence staining. To evaluate the effects of FASN expression on HCV replication, Huh7/Rep-Feo cells were seeded at a density of 1×10^4/well. Then 2 μg of pCMV3B-FASN or the pCMV3B vector control plasmid was transfected into the cells by use of LF2000. At 48 h after transfection, the luciferase activity was quantified using the Bright-Glo luciferase assay reagent. For lentivirus-mediated knockdown of FASN, HEK293 cells were seeded at a density of 2×10^6/60-mm culture dish for 24 h. Then 4 μg of the indicated pLKO.1-shRNA (Fig. 5) and 4 μg of pCMVdR and pMD2.G were transfected into HEK293 cells by use of the Arrest-In transfection reagent. At 4 h after transfection, the supernatant was removed and was replaced by fresh medium. The virus-containing supernatants collected at 24 and 36 h after transfection were combined and clarified by low-speed centrifugation, passed through a filter (pore size, 0.45 μm), and stocked at −80°C for further use.

Immunoprecipitation assay. The cells were dissolved in EBC lysis buffer (125 mM NaCl, 50 mM Tris-HCl [pH 7.4], 0.5 mM EDTA, 0.25% Nonidet P-40, 10 μg/ml aprotinin, 10 μg/ml leupeptin, 1 mM phenylmethylsulfonyl fluoride [PMSF], 200 μM sodium orthovanadate, 10 mM sodium fluoride, and 100 μM EGTA) and were incubated on ice for 30 min. Subsequently, the lysates were clarified by centrifugation at 13,000 rpm for 2 min. The protein extracts were then incubated with 2 μg of the indicated antibody or control IgG at 4°C for 2 h. Protein A Sepharose beads were then added and were incubated at 4°C for 4 h. The immunoprecipitated complexes were washed three times with radioimmunoprecipitation assay (RIPA) buffer (0.15 M NaCl, 0.01 M sodium phosphate [pH 7.2], 50 mM sodium fluoride, 0.2 mM sodium vanadate, 1% sodium deoxycholate, 0.1% SDS, 1% NP-40, 2 mM EDTA, and 100 U/ml aprotinin). The protein complexes were then separated by 8% SDS-PAGE for Western blot analysis using the enhanced chemiluminescence (ECL) kit as described previously (20).

Immunofluorescence staining. The cells were washed twice with 1× PBS and fixed with 4% paraformaldehyde at room temperature for 20 min. After permeabilization by 0.2% Triton X-100 on ice for 20 min, the permeable cells were incubated with 4% bovine serum albumin (BSA) at 37°C for 1 h. The cells were then incubated with the indicated antibody for 1 h at room temperature and were subsequently detected by an Alexa 488-conjugated anti-mouse secondary antibody or a rhodamine-conjugated anti-rabbit secondary antibody for 1 h. The fluorescence-labeled proteins were observed with a Leica TCS SP2 confocal microscope and were analyzed in the *x-z* and *y-z* sections. The colocalization coefficient for the cell images ($n = 10$) were calculated with MetaMorph software (version 7.0; Molecular Devices) (20).

RNA isolation and real-time quantitative RT-PCR. Total RNA was isolated by REzol C & T RNA extraction reagent as described by the manufacturer (Protech, Taipei, Taiwan). For the quantification of HCV RNA expression, total cellular RNA (100 ng) was subjected to one-step reverse transcription-PCR (RT-PCR) in a 25-μl reaction mixture containing 2× SYBR green PCR Master Mix with the primer set for HCV (HCV-F, 5′-TGCGGAACCGGTGAGTACA-3′; HCV-R, 5′-CTTAAGGTTTAGGATTCGTGCTCAT-3′) or the primer set for FASN (FASN-F, 5′-GAAACTGCAGGAGCTGTCC-3′; FASN-R, 5′-CACGGAGTTGAGCCGCAT-3′). The reaction conditions were as follows: 1 cycle of 48°C for 30 min, 1 cycle of 95°C for 10 min, and 40 cycles of 95°C for 15 s and 60°C for 1 min, by use of the ABI Prism 7000 sequence detection system.

The method for detecting the minus strand of HCV RNA was modified from that in a previous report (22). In brief, the cDNA was generated with a Taq-149 primer (5′-ACATGCGCGGCATCTAGATGCGGAACCGGTGAGTACA-3′) using Moloney murine leukemia virus (M-MLV) reverse transcriptase and was subsequently quantified by real-time PCR with a 25-μl reaction mixture containing 2× SYBR green PCR Master Mix and a primer set consisting of Taq (5′-ACATGCGCGGCATCTAGA-3′) and HCV-R. The reaction conditions were as follows: 1 cycle of 95°C for 10 min, followed by 40 cycles of 95°C for 15 s and 60°C for 1 min, by use of the ABI Prism 7000 sequence detection system. The expression of β-actin was used as a normalization control. HCV RNA expression was quantified using the $\Delta\Delta C_T$ method, where C_T represents the threshold cycle.

Infectious HCV particle production and infection inhibition assay. Infectious HCV particles (HCVcc) were produced as described previously (23, 24). Briefly, *in vitro*-transcribed genomic JC1-Luc2A RNA was delivered into Huh7.5.1 cells by electroporation. The JC1-Luc2A HCV reporter virus was recovered from cell culture medium. The virus-containing supernatant was clarified by low-speed centrifugation, passed through a 0.45-μm-pore-size filter, and concentrated by ultracentrifugation. For the infection inhibition assay, Huh7.5.1 cells were seeded in 24-well plates at a density of 5×10^4/well. Twenty-four hours later, the cells were infected with a lentivirus carrying shFASN in the presence of Polybrene (8 μg/ml) for 24 h. The virus-containing supernatant was then removed, and fresh medium with puromycin was added for an additional 48 h. The FASN knockdown cells were then seeded in 96-well plates at a density of 1×10^4/well. At 24 h after plating, the HCV reporter virus (multiplicity of infection [MOI], 0.1) was added to each well for 24 h. The virus-containing supernatant was then removed and was replaced with fresh medium for an additional 96 h. The cell lysates were then collected for further analyses as indicated.

Membrane flotation assay. The membrane flotation assay was performed as described previously (25). Briefly, Huh7/Rep-Feo cells were harvested in 100 μl of hypotonic buffer (10 mM Tris-HCl [pH 7.5], 10 mM KCl, and 5 mM $MgCl_2$) and were incubated for 30 min on ice. The cell lysates were passed through a 26-gauge needle, followed by centrifugation at $1{,}000 \times g$ for 5 min at 4°C. One milligram of the cell lysate was either left untreated or treated with 1% NP-40 on ice for 1 h before the application of a 10%-to-72% sucrose gradient at 38,000 rpm for 14 h at 4°C (Hitachi S55S rotor). Two hundred microliters of each fraction was collected from the top to the bottom, and the fractions were subsequently separated by 10% SDS-PAGE.

Preparation of CRC. Crude replication complexes (CRC) were prepared as described previously (26). Briefly, the cells were suspended in hypotonic buffer (10 mM Tris-HCl [pH 7.5], 10 mM KCl, 1.5 mM $MgCl_2$, 0.5 mM PMSF, and 2 μg/ml aprotinin) and were passed through a 26-gauge needle. Cell debris was removed by centrifugation at $1{,}000 \times g$ for 10 min, and the supernatant (S1) was collected. The S1 supernatant was further centrifuged at $69{,}000 \times g$ for 1 h at 4°C (Hitachi S55S rotor). The supernatant (S2) and pelleted CRC were collected. To understand if FASN is located in the CRC with HCV NS5B, CRC were treated with 1 mg/ml proteinase K (total volume, 100 μl) at 37°C for 5 min. The proteinase K-treated CRC were concentrated by adding 25 μl of TCA (containing 1 mM PMSF), followed by centrifugation at 13,000 rpm for 10 min. The pellet was washed with cold acetone twice at 13,000 rpm for 10 min each time and was then dried at 95°C for 10 min, followed by protein fractionation using 10% SDS-PAGE. In parallel, an equal amount of CRC was incubated with 2 U/μl of S7 nuclease at 37°C for 15 min, and the reaction was stopped with 10 mM EGTA. The reaction activity was confirmed by the detection of 28S RNA, and the HCV RNA level was quantified by real-time RT-PCR and an *in vitro* replicase activity assay as described previously (26). Briefly, the reaction mixture, containing 20 mM Tris-HCl (pH 7.5), 10 mM $MgCl_2$, 5 mM dithiothreitol, 5 mM KCl, 40 μg/ml of actinomycin D, 20 μCi of [α-^{32}P]CTP, 10 μM CTP, 1 mM (each) ATP and UTP, 5 mM GTP, 2.5 mM phosphoenolpyruvate, 1 U of RNasin, and 1 U of pyruvate kinase in a total volume of 20 μl, was incubated at 35°C for 60 min. The reaction products were purified by phenol-chloroform ex-

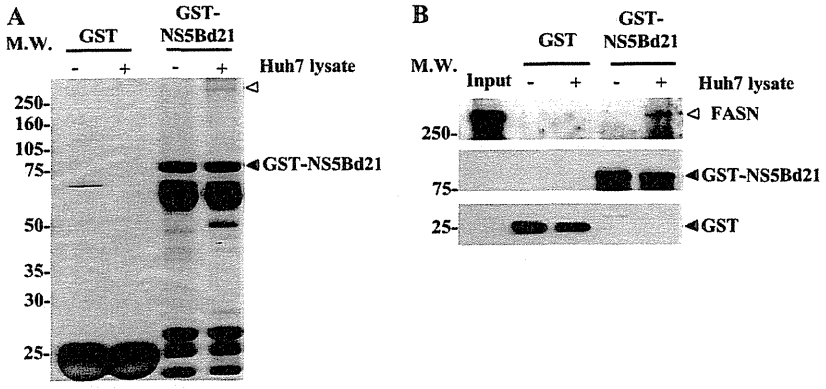

FIG 1 FASN interacts with NS5B. (A) GST and GST-NS5B fusion proteins (GST-NS5Bd21) were purified with glutathione Sepharose 4B beads for a pulldown assay in the absence (−) or presence (+) of Huh7 cell lysates. Equal volumes of purified fusion proteins and pulldown proteins were separated by 10% SDS-PAGE, followed by silver staining. The open arrowhead indicates the candidate protein that specifically bound to GST-NS5Bd21. MW, molecular weight (in thousands). (B) Pulled down proteins were analyzed by Western blotting using anti-FASN (top), anti-NS5B (center), and anti-GST (bottom) antibodies. Accordingly, FASN was confirmed to interact with NS5B. Input, 1/30 of the Huh7 cell lysates used for GST pulldown.

traction and isopropanol precipitation, followed by denaturing agarose gel electrophoresis. The radioactive signal was detected and analyzed by phosphorimaging using the Typhoon Trio 9410 instrument (GE Healthcare).

Protein purification. Histidine-tagged proteins were purified with Ni-nitrilotriacetic acid (NTA) His·Bind resin (Novagen, Darmstadt, Germany). For His-FASN, pcDNA3.1 HisC-FASN was transfected into HEK293 cells, and 1 mg of the collected cell lysates was incubated with His·Bind resin at 4°C for 1.5 h. The protein was then eluted with 200 mM imidazole. For the production of recombinant NS5B, the pET32a-NS5Bd21 plasmid was transformed into *E. coli* BL21(Lys), followed by induction with 1 mM IPTG at 20°C for 24 h. Subsequently, the bacterial suspension was centrifuged (13,000 rpm) at 4°C for 1 h. The His-NS5B proteins that were present in the supernatant were eluted with 200 mM imidazole and were concentrated using an Amicon Ultra-4 50K centrifugal filter unit (Millipore, Bedford, MA).

RdRp activity assay. The RNA-dependent RNA polymerase (RdRp) activity assay was performed as described previously with minor modifications (27). Briefly, the reaction reagents were added to a 96-well plate with a final volume of 100 μl/well in the following order. At first, reaction buffer A [0.5 μg/ml oligo(G_{12}) and 5 μg/ml poly(C)] was preincubated at room temperature for 10 min. In parallel, reaction buffer B (20 mM HEPES [pH 7.3], 7.5 mM DTT, 20 U/ml RNAsin, 1 μM GTP, 10 mM $MgCl_2$, 5 mM NaCl, and 100 μg/ml BSA) was prepared and was mixed with buffer A. Then reaction buffer C (0.03 U/ml ATP sulfurylase, 0.5 mM coenzyme A, 310 μM D-luciferin, and 5 μM adenosine 5′-phosphosulfate) was added to the reaction mixtures. Finally, the enzyme mixture (250 nM NS5B and 1 nM luciferase) was added to the well, and RdRp activity was detected by a SpectraMax microplate reader (Molecular Devices).

RESULTS

FASN is identified as an NS5B-interacting protein by proteomic and MALDI-TOF analysis. To elucidate the mechanisms underlying HCV replication and to explore the interplay between viral and host factors, we attempted to identify proteins interacting with HCV RNA polymerase NS5B in the lysates of Huh7 cells, a cell line well known for its ability to facilitate HCV RC formation and viral production. A GST fusion protein, GST-NS5Bd21, lacking the C-terminal 21 amino acids of NS5B, was used as the bait to pull down NS5B-interacting proteins. After protein fractionation by SDS-PAGE and silver staining, a candidate protein with a molecular size of approximately 250 kDa was present in the pulldown lysates of GST-NS5Bd21 but not in those of the control protein GST (Fig. 1A). The identity of the candidate protein was unveiled by spectrum analysis of the peptide profiles generated by MALDI-TOF MS. With 18% sequence coverage, the protein was identified as the lipogenic enzyme FASN (see Table S1 in the supplemental material). The calculated molecular mass of FASN is 276 kDa, which is consistent with the location of the candidate protein on SDS-PAGE gels. Western blot analysis of the GST-NS5Bd21 pulldown lysates using an anti-FASN antibody further confirmed FASN as the NS5B-interacting protein (Fig. 1B).

NS5B-FASN interaction is mediated by the N terminus of NS5B. To determine whether FASN interacts directly with NS5B in the absence of other viral proteins, FASN and NS5B expression plasmids were cotransfected into 293T cells, followed by immunoprecipitation with an anti-FASN antibody. Western blot analysis using an anti-NS5B antibody revealed that NS5B was present in protein complexes immunoprecipitated by the anti-FASN antibody but not by the IgG control antibody (Fig. 2A), implying that other viral proteins do not contribute to the interaction of NS5B and FASN.

To define the region of NS5B that mediates its interaction with FASN, serial NS5B deletion mutants (Fig. 2B) were generated and were coexpressed with FASN in 293T cells. After immunoprecipitation with an anti-FASN antibody, Western blot analyses were performed to determine whether NS5B mutant proteins were present in FASN-immunoprecipitated protein complexes (Fig. 2C). Like NS5B/1-570, both NS5B/1-180 and NS5B/1-335 were able to bind FASN. In contrast, the FASN binding activity of NS5B was abrogated by deleting amino acids 1 to 178 (NS5B/179-570). In agreement with these findings, FASN can be detected in the immunoprecipitated protein complexes of full-length NS5B but not in those of NS5B/179-570 (Fig. 2D). These data suggest that the first 178 amino acids, where the finger domain of NS5B is located (28), play a pivotal role in mediating the binding of NS5B to FASN.

FASN interacts with NS5B in HCV subgenomic replicon cells and HCVcc-infected cells. To confirm the interaction between endogenous FASN and NS5B, HCV subgenomic replicon cells were subjected to coimmunoprecipitation and immunofluorescence staining assays. The subgenomic replicon cell lysates were immunoprecipitated with an anti-FASN antibody, fol-

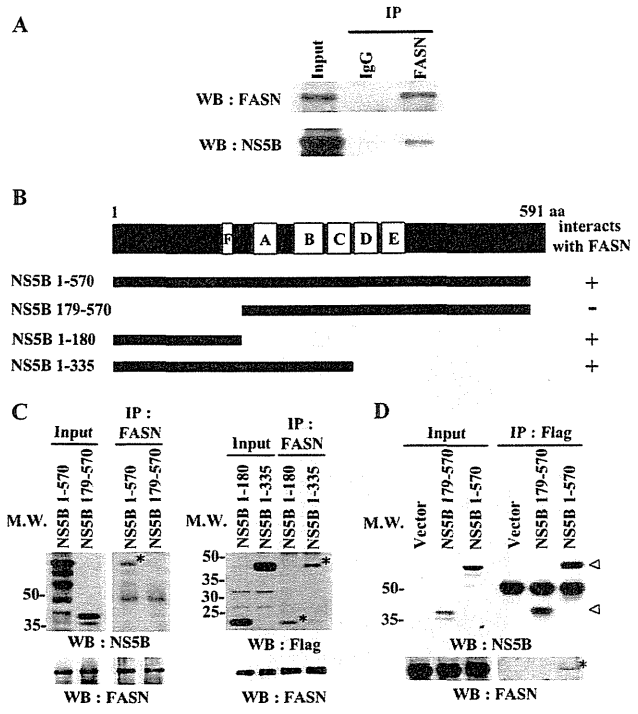

FIG 2 FASN binds to the N terminus of NS5B. (A) The NS5B and FASN expression plasmids were cotransfected into HEK293T cells, followed by immunoprecipitation (IP) with an anti-FASN antibody. The immunoprecipitated proteins were detected by Western blotting (WB) using an anti-FASN or anti-NS5B antibody. (B) Schematic representation of the NS5B deletion mutants. The six motifs essential for the RNA-dependent polymerase are denoted as A to F. (C) Expression plasmids for the indicated NS5B deletion mutants were cotransfected with the FASN expression plasmid into HEK293T cells. At 48 h after transfection, immunoprecipitation was performed using an anti-FASN antibody, and NS5B was detected by Western blotting using an anti-NS5B or anti-Flag tag antibody. Asterisks indicate the binding of NS5B to FASN. MW, molecular weight (in thousands). (D) The FASN expression plasmid was cotransfected with the indicated NS5B expression plasmids into HEK293T cells. At 48 h after transfection, immunoprecipitation was performed using an anti-Flag tag antibody, and FASN was detected by Western blotting using an anti-FASN antibody. Open arrowheads indicate the NS5B deletion mutant proteins. The asterisk indicates the binding of FASN to NS5B.

lowed by Western blotting of the HCV proteins. Our data revealed that NS5B and NS5A, but not NS3, were present in the immunocomplexes of FASN (Fig. 3A). The interaction between NS5B and FASN still occurred when immunoprecipitation was performed using lysates from Huh7 cells coexpressing FASN and NS5B expression plasmids. However, NS5A was not detectable in the immunocomplexes of FASN when FASN and NS5A were coexpressed in Huh7 cells (Fig. 3B). In addition, a coimmunoprecipitation assay of the HCVcc-infected Huh7.5.1 cell lysates using an anti-FASN antibody further confirmed the interactions of NS5B and FASN (Fig. 3C). These data not only define the interactions between FASN and NS5B but also suggest that FASN, likely through NS5B, interacts with other HCV proteins, such as NS5A, and forms large protein complexes with them.

To further demonstrate the interaction between FASN and NS5B, Huh7/Rep-Feo subgenomic replicon cells and HCVcc-infected Huh7.5.1 cells were subjected to immunofluorescence staining using a rabbit anti-NS5B or mouse anti-FASN antibody. NS5B was found to be distributed mostly near the perinuclear region, whereas FASN was found in the cytoplasm. The merged images at the *x-z* and *y-z* sections revealed that FASN and NS5B were colocalized in the perinuclear region, with a colocalization coefficient of 80% (Fig. 3D), supporting the notion that FASN is an NS5B-interacting protein.

NS5B protein is usually associated with the detergent-resistant lipid raft membrane fraction (29). To determine whether FASN and NS5B colocalize in the lipid rafts of Huh7/Rep-Feo cells, the lysates were extracted in the absence or presence of 1% NP-40 and were fractionated by a 10-to-72% sucrose gradient. Each fraction of the gradient was collected for Western blot analysis. Fractions 2 and 3 were considered lipid rafts based on the presence in these fractions of caveolin-2, a lipid raft membrane protein resistant to 1% NP-40 solubilization (25), regardless of whether the cell lysates were extracted in the presence or absence of NP-40. On the other hand, GRP78, an ER marker not associated with lipid rafts and sensitive to 1% NP-40 solubilization (25), was detectable in the bottom of the gradient and was not detected in the detergent-resistant membrane fractions. In agreement with previous studies (29), the viral protein NS5B was associated with lipid raft fractions in the sucrose gradient (Fig. 3E, top). Portions of FASN protein were codistributed with NS5B in lipid rafts (Fig. 3E, top). Notably, the distribution of FASN in lipid rafts was not observed in Huh7 cells that did not express any HCV proteins (Fig. 3E, bottom). These results suggest that FASN was recruited by HCV proteins, most likely through the interaction with NS5B, into lipid rafts.

Inhibition of FASN activity decreases HCV protein and RNA expression levels. The interaction of FASN with HCV NS5B may be involved in the regulation of HCV proteins and RNA expression. To elucidate whether there is a correlation between FASN expression and the infectivity of HCV, FASN expression in HCV-permissive Huh7.5.1 cells was compared with that in the parental Huh7 cells. Real-time RT-PCR analysis revealed that FASN mRNA expression was higher in HCV-permissive Huh7.5.1 cells than in Huh7 cells (Fig. 4A, left) ($P < 0.01$). In agreement with these observations, FASN expression was also increased in HCVcc-infected (MOI, 3) Huh7.5.1 cells (Fig. 4A, right) ($P < 0.05$). These data suggest that FASN expression likely facilitates HCV infection and replication.

The lipid raft is the major cellular compartment for the assembly of HCV RC. The colocalization of FASN and NS5B in the lipid raft led us to delineate the role of FASN in HCV replication. First, subgenomic replicon cells were treated with C75, an inhibitor of the β-ketoacyl synthase domain of FASN (30), to inhibit cellular FASN activity. Western blot analysis revealed that C75 had no effect on FASN expression but caused a decrease in the expression of NS5A and NS5B from that for the untreated control or cells treated with the solvent dimethyl sulfoxide (DMSO) (Fig. 4B, left). In agreement with these findings, HCV RNA expression was also inhibited by C75 in a dose-dependent manner, with 34% and 68% inhibition at the noncytotoxic concentrations of 20 and 40 μM, respectively (Fig. 4B, center and right).

The subgenomic replicon cells were also treated with orlistat, an inhibitor of the thioesterase domain of FASN and an FDA-approved drug used for treating obesity (31), to elucidate FASN function in viral replication. The expression levels of HCV RNA, as reflected by luciferase activity in Huh7/Rep-Feo cells, were determined. At the dosage of the 50% effective concentration (EC_{50}) (50 μM), which is noncytotoxic, orlistat caused a 45% decrease in

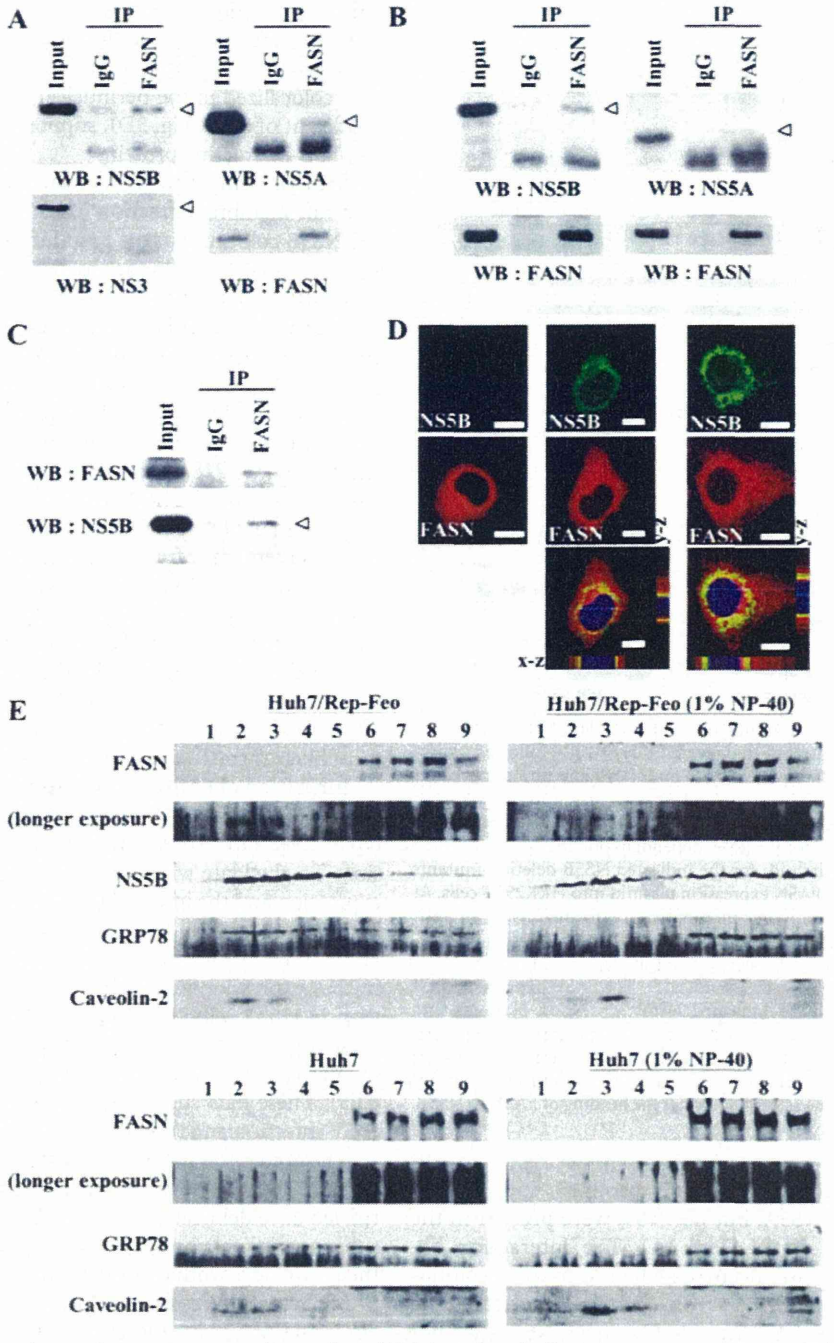

FIG 3 NS5B interacts and colocalizes with FASN in HCV replicon cells and HCVcc-infected cells. (A) Immunoprecipitation (IP) of subgenomic replicon cell lysates was performed with an anti-FASN antibody. The immunoprecipitated proteins were analyzed by Western blotting (WB) with an anti-NS5B, anti-NS5A, anti-NS3, or anti-FASN antibody. (B) Huh7 cells were cotransfected with plasmids expressing FASN and NS5B (left) or FASN and NS5A (right) for 48 h. The transfected cell lysates were then immunoprecipitated using an anti-FASN antibody. NS5B or NS5A was subsequently detected by Western blotting using an anti-NS5B or anti-NS5A antibody, respectively. (C) Huh7.5.1 cells were infected with JC1-Luc2A HCVcc (MOI, 3). After infection for 72 h, the infected-cell lysates were collected for immunoprecipitation with an anti-FASN antibody. The immunoprecipitated proteins were analyzed by Western blotting using an anti-NS5B or anti-FASN antibody. (D) Immunofluorescence staining of Huh7 cells (left), subgenomic replicon cells (center), and Huh7.5.1 cells infected with JC1-Luc2A HCVcc (MOI, 3) (right) was performed using anti-FASN and anti-NS5B antibodies. The rhodamine- or Alexa 488-conjugated secondary antibody was then used to visualize the FASN or NS5B protein, respectively. The cell images were captured using a Leica SP2 confocal spectral microscope. The images of the *x-z* section and the *y-z* section were acquired from the dashed lines from the center *x-y* panel of the bottom merged image. The yellow area indicates the colocalization of NS5B with FASN. Bars, 10 μm. (E) Huh7/Rep-Feo and Huh7 cell lysates were harvested in parallel with a hypotonic buffer and were either left untreated or mixed with 1% NP-40 for 1 h on ice. The lysate was fractionated by a 10-to-72% sucrose gradient at 38,000 rpm for 14 h. After centrifugation, the sample was separated into nine fractions, which were analyzed by Western blotting with the indicated antibodies.

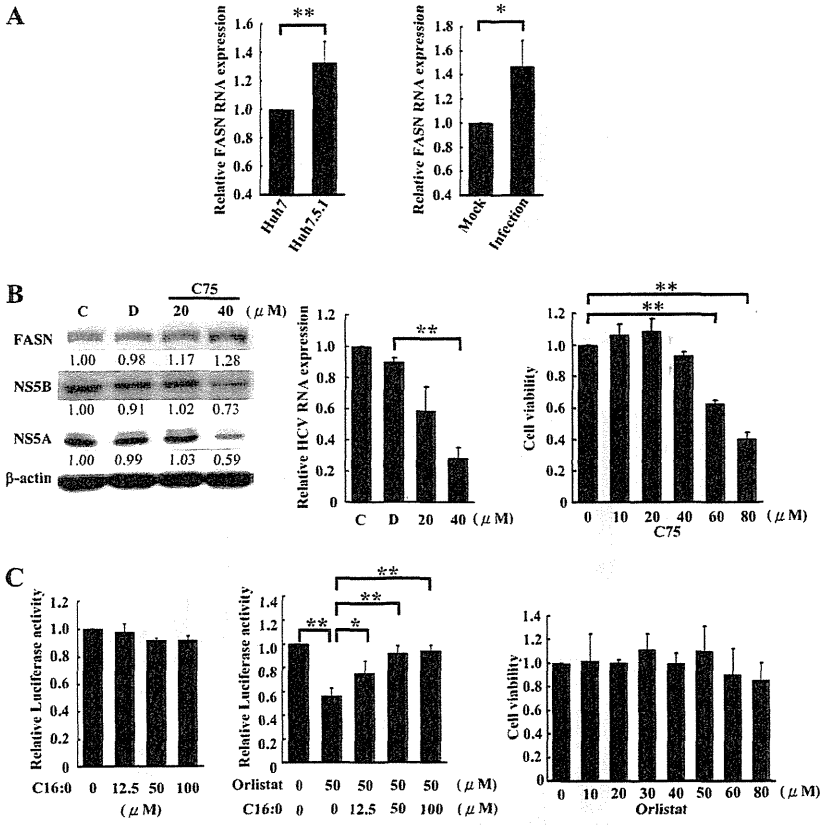

FIG 4 FASN activity is required for HCV replication. (A) Cellular RNAs from the indicated cells (left) or mock- or JC1-Luc2A HCVcc-infected Huh7.5.1 cells (right) were collected for real-time RT-PCR to analyze FASN mRNA expression. (B) (Left) HCV subgenomic replicon cells were treated with the FASN inhibitor C75 for 48 h. The cell lysate was harvested, and Western blot analysis was performed using the indicated antibodies. The ratios for the relative band intensities of each indicated protein normalized by β-actin are shown. C, control untreated cells; D, DMSO-treated cells. (Center) In parallel, cellular RNA was collected, and viral RNA was detected by real-time RT-PCR. The expression of glyceraldehyde-3-phosphate dehydrogenase was used as a control for normalization. The expression level for untreated cells was arbitrarily set at 1. Data are means ± standard deviations ($n = 3$; **, $P < 0.01$). (Right) The viability of HCV subgenomic replicon cells treated with the indicated concentrations of C75 was measured by an MTS assay. Data are means ± standard deviations ($n = 3$; **, $P < 0.01$). (C) (Left and center) Huh7/Rep-Feo cells were treated with the indicated concentrations of palmitate ($C_{16:0}$) (left) or the FASN inhibitor orlistat combined with the indicated dose of palmitate for 72 h (center). Luciferase activities were determined, and the relative luciferase activity is shown. The luciferase activity for the negative control was arbitrarily set at 1. Data are means ± standard deviations ($n = 3$; *, $P < 0.05$; **, $P < 0.01$). (Right) The viability of HCV Huh7/Rep-Feo cells treated with the indicated concentrations of orlistat was measured by an MTS assay. Data are means ± standard deviations ($n = 3$).

luciferase activity (Fig. 4C, center and right). Although palmitate (C16:0), the principal product of FASN, had no effect on HCV expression alone (Fig. 4C, left), the suppressive effect of orlistat on HCV RNA expression could be abrogated in a dose-dependent manner by cotreatment with palmitate (C16:0) (Fig. 4C, middle panel). These data suggest that FASN activity is important for HCV replication.

Abrogation of FASN expression diminishes HCV expression and replication. To further delineate the role of FASN in HCV expression and replication, FASN was overexpressed in Huh7/Rep-Feo cells, and the luciferase activity, corresponding to the level of HCV RNA expression, was analyzed (Fig. 5A, left). In FASN-overexpressing cells, luciferase activity was increased 2.4-fold over that in control vector-transfected cells ($n = 3$; $P < 0.05$). In agreement with these findings, knockdown of FASN in the replicon cells by small interfering RNA (siF) caused a 44% decrease in luciferase activity from that in cells transfected with nontargeting control small interfering RNA (siG) (Fig. 5A, right). Moreover, the expression levels for total and negative-strand HCV RNA were decreased by 41% and 42%, respectively, in siF-transfected subgenomic replicon cells (Fig. 5B).

To elucidate whether FASN has any functional impact on HCVcc production, Huh7.5.1 cells were transfected with the JC1-Luc2A-based HCV reporter virus (MOI, 0.1) and were infected with a lentivirus encoding shFASN (shFASN-C or shFASN-D). As indicated by Western blotting and immunofluorescence staining analyses, Huh7.5.1 cells expressing either of the shFASN constructs exhibited a 65% decrease in the level of HCV core protein (Fig. 5C). In agreement with these findings, the luciferase activity reflecting the level of HCVcc production was decreased by approximately 60% (Fig. 5D, top). Moreover, when the supernatants from shFASN-C- or shFASN-D-transduced HCVcc-infected cells were collected to reinfect naïve Huh7.5.1 cells, the luciferase activity of the reinfected cells was decreased by 83% or 43%, respectively (Fig. 5D, bottom). These data suggest that FASN expression modulates HCV replication and affects viral production.

FASN is a component of HCV replication complexes and modulates NS5B RdRp activity. Previous study has indicated that

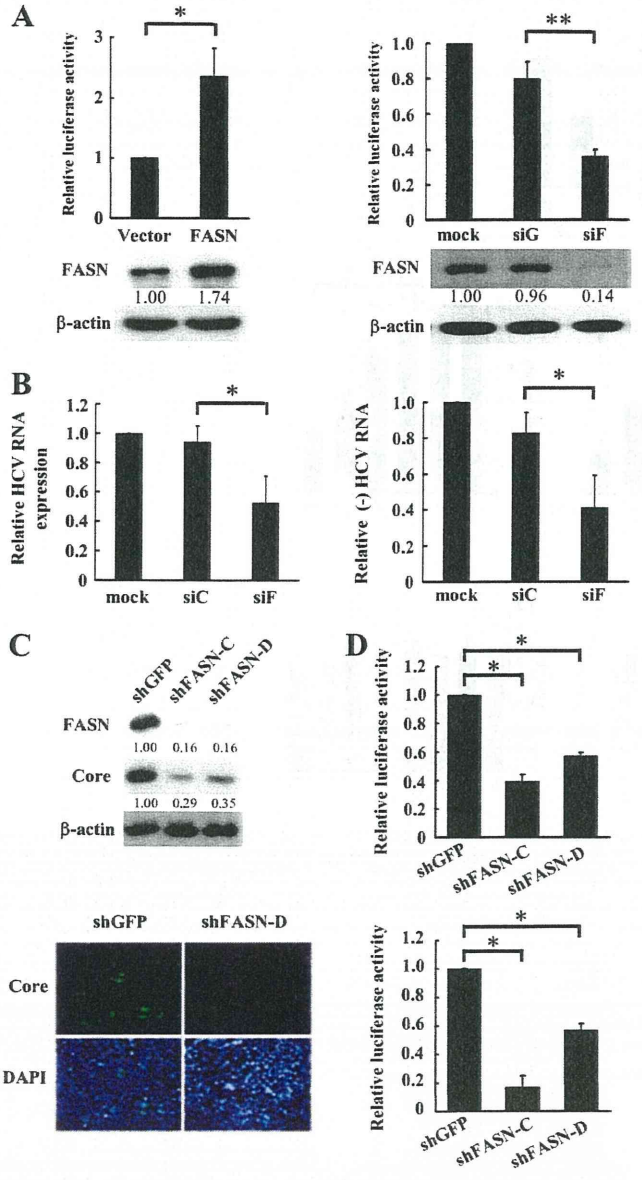

FIG 5 FASN expression is required for HCV replication. (A) Huh7/Rep-Feo cells were transfected with an FASN expression plasmid (left) or a siFASN oligonucleotide (siF) (right) for 48 h. Mock-transfected or siGFP-transfected (siG) cells were used as controls for the FASN knockdown experiment. The luciferase activities were determined, and Western blot analysis was performed in parallel to determine the level of FASN expression. The ratios for the relative band intensity of FASN after normalization with β-actin are shown. The ratio for the vector control or for mock transfection was arbitrarily set at 1. Luciferase activities are means ± standard deviations for three independent experiments (*, $P < 0.05$; **, $P < 0.01$). (B) The expression levels of total and minus-strand (−) HCV RNA for Huh7/Rep-Feo cells with FASN knockdown were determined by real-time RT-PCR. The expression of glyceraldehyde-3-phosphate dehydrogenase was used as a control for normalization. The expression level for mock-transfected cells was arbitrarily set at 1. siC is a nontargeting siRNA control. Data are means ± standard deviations for three independent experiments (*, $P < 0.05$). (C) Huh7.5.1 cells were seeded in 24-well plates at a density of 5×10^4/well for 24 h and were infected with a lentivirus carrying shGFP or shFASN (shFASN-C and shFASN-D). The cells were then seeded in a 96-well plate at a density of 1×10^4/well, followed by infection with the JC1-Luc2A HCV reporter virus (MOI, 0.1). The infected cells were fixed and stained with an anti-HCV core antibody. In parallel, the cell lysates were collected to determine the expression of FASN and HCV core proteins by Western blotting. (D) (Top) The HCV infectivity of the cells was measured by a luciferase activity assay. (Bottom) The viruses in the infected-cell supernatants were collected and used to reinfect naïve Huh7.5.1 cells. The reinfected cell lysates were collected, and the luciferase activities were determined. Data are means ± standard deviations for three independent experiments (*, $P < 0.05$).

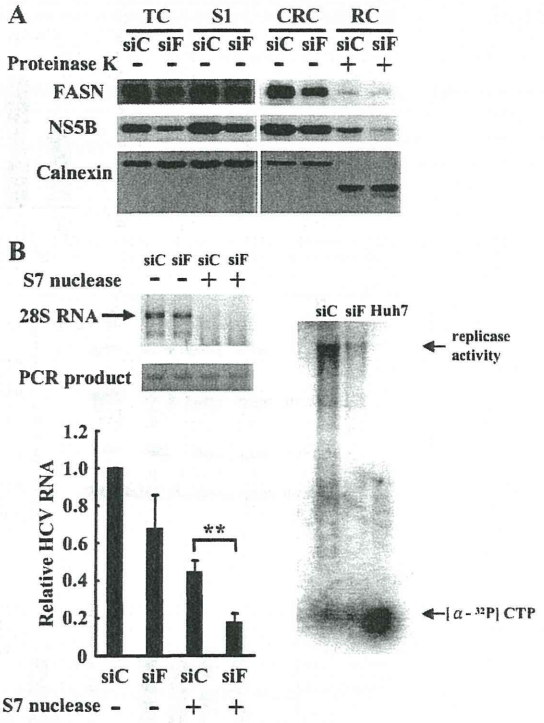

FIG 6 Fatty acid synthase is a component of the HCV replication complex. (A) Subgenomic replicon cells were transfected with a control (siC) or siFASN (siF) oligonucleotide. CRC were isolated from the cell lysates as described in Materials and Methods. The presence of the indicated proteins in the total-cell lysate (TC), supernatant (S1), CRC, and proteinase K-treated CRC (RC) was analyzed by Western blotting. (B) (Left) The RNA from the CRC fractions of the indicated transfected cells, either left untreated or treated with S7 nuclease, was analyzed by agarose gel electrophoresis for the expression levels of 28S RNA and by real-time RT-PCR for HCV RNA expression. The expression level for cells transfected with the nontargeting siRNA control (siC) without S7 nuclease treatment was arbitrarily set at 1. Data are means ± standard deviations for three independent experiments (**, $P < 0.01$). (Right) The *in vitro* replicase activity of S7 nuclease-resistant RC for the indicated cell lines was analyzed, and the reaction products were analyzed by denaturing agarose gel electrophoresis, followed by phosphorimaging of the dried gel. The major reaction product of the *in vitro* replicase assay is indicated by an arrow.

NS5B is present in HCV RC that are formed by invaginations of cholesterol- and sphingomyelin-rich membranes during replication. Due to the vesicular membrane structures, the complexes are resistant to protease and nuclease treatment (26). Considering the functional role of FASN in viral replication and the interplays between FASN and NS5B, we first investigated whether FASN is present in RC and then employed siF- and siC-transfected replicon cells to delineate the effects of FASN knockdown on the activity of RC. The total-cell lysate, supernatant (S1), CRC, and proteinase K-treated CRC (RC) were prepared from both siF- and siC-transfected cells. Western blot analyses revealed that FASN was present in both CRC and RC and that, together with NS5B, it